IMMUNOLOGY

A dominant function of LynB kinase in preventing autoimmunity

Ben F. Brian IV[1]†‡, Monica L. Sauer[2]†, Joseph T. Greene[3]†, S. Erandika Senevirathne[1], Anders J. Lindstedt[4,5], Olivia L. Funk[3], Brian L. Ruis[6], Luis A. Ramirez[3], Jennifer L. Auger[7], Whitney L. Swanson[3]§, Myra G. Nunez[3], Branden S. Moriarity[6,8,9,10], Clifford A. Lowell[11], Bryce A. Binstadt[7,12], Tanya S. Freedman[3,9,12,13]*

Here, we report that the LynB splice variant of the Src-family kinase Lyn exerts a dominant immunosuppressive function in vivo, whereas the LynA isoform is uniquely required to restrain autoimmunity in female mice. We used CRISPR-Cas9 gene editing to constrain *lyn* splicing and expression, generating single-isoform LynA knockout (LynA^{KO}) or LynB^{KO} mice. Autoimmune disease in total Lyn^{KO} mice is characterized by production of antinuclear antibodies, glomerulonephritis, impaired B cell development, and overabundance of activated B cells and proinflammatory myeloid cells. Expression of LynA or LynB alone uncoupled the developmental phenotype from the autoimmune disease: B cell transitional populations were restored, but myeloid cells and differentiated B cells were dysregulated. These changes were isoform-specific, sexually dimorphic, and distinct from the complete Lyn^{KO}. Despite the apparent differences in disease etiology and penetrance, loss of either LynA or LynB had the potential to induce severe autoimmune disease with parallels to human systemic lupus erythematosus (SLE).

INTRODUCTION

The Src-family kinase (SFK) Lyn catalyzes the activation of many immune cell signaling pathways, including initiating antimicrobial responses by phosphorylating ITAMs [immunoreceptor tyrosine-based activation motifs; e.g., in B cell antigen receptor (BCR) and myeloid cell Fc gamma receptor (FcγR)] (*1*–*6*). However, Lyn can also perform inhibitory functions downstream of ITAMs and Toll-like receptors (TLRs) in B and myeloid cells. To suppress ITAM signaling, Lyn phosphorylates ITIMs (immunoreceptor tyrosine-based inhibitory motifs; e.g., in CD22 and SIRPα) and tyrosine and lipid phosphatases (e.g., SHP-1 and SHIP1) (*2*, *7*, *8*). Catalytic and adaptor functions of Lyn can suppress TLR signaling via SHIP1, the phosphatidylinositol kinase PI3K, and the transcription factor IRF5 (*9*–*12*).

In humans, hypomorphic alleles of *LYN* are linked to systemic lupus erythematosus (SLE) (*13*, *14*); in addition, lupus patients often have functional deficiencies in Lyn expression, signaling, or trafficking (*15*, *16*). With age, Lyn knockout (Lyn^{KO}) mice develop an autoimmune disorder with similarities to human SLE, including antinuclear antibody (ANA) production, glomerulonephritis, myeloproliferation, splenomegaly, B cell lymphopenia, and selective enrichment of autoreactive and inflammatory B cell and myeloid cell subsets (*17*–*19*). While Lyn functions in multiple cell types to suppress autoimmunity, it is not clear how the opposing positive and negative functions of Lyn are integrated in different populations of myeloid and B cells and signaling pathways to maintain immune homeostasis (*5*, *6*).

Although no sex-specific differences have been reported in Lyn^{KO} mice, 90% of human SLE patients are women (*20*). The reasons for this disparity are still a matter of discussion, with genetic and environmental factors both likely contributors. Hormone signaling appears to be involved, as SLE symptoms worsen during pregnancy (*21*). Immune cells express estrogen and androgen receptors, allowing them to respond directly to sex hormones. In addition, women can have higher inflammatory set points, with higher type I interferon (IFN) and antibody titers and more frequent allograft rejection (*22*–*25*). Incomplete X-chromosome inactivation in immune cells (*26*, *27*), leading to increased protein levels of TLR7, Bruton's tyrosine kinase, and CD40L (*23*), may also be a factor predisposing women to SLE and other autoimmune diseases. Higher levels of TLR7 in B cells, monocytes, and plasmacytoid dendritic cells (pDCs) can lead to increased inflammatory signaling and production of IgD^{-}CD27^{-} double negative (DN2) B cells in women or aging-associated B cells (ABCs) in female mice (*27*–*31*). It is not known whether Lyn^{KO} mice lack a sex-specific driver of lupus or whether the resulting disease, which can be initiated by conditional deletion of Lyn in either B cells or DCs alone (*11*, *32*), is simply so severe as a germline knockout that it obscures any sex differences. The molecular mechanisms regulating Lyn function in a sex- and cell-specific manner are also unclear.

Lyn is expressed as two isoforms: LynA (56 kDa) and LynB (53 kDa). Spliced from a 5′ alternative donor site within exon 2, LynB lacks a 21–amino acid insert present in LynA (Fig. 1A and fig. S1A) (*33*). Using overexpression/reconstitution approaches in

[1]Graduate Program in Molecular Pharmacology and Therapeutics, University of Minnesota, Minneapolis, MN 55455, USA. [2]Graduate Program in Biochemistry, Molecular Biology, and Biophysics, University of Minnesota, Minneapolis, MN 55455, USA. [3]Department of Pharmacology, University of Minnesota, Minneapolis, MN 55455, USA. [4]Graduate Program in Microbiology, Immunology, and Cancer Biology, University of Minnesota, Minneapolis, MN 55455, USA. [5]Medical Scientist Training Program, University of Minnesota, Minneapolis, MN 55455, USA. [6]Center for Genome Engineering, University of Minnesota, Minneapolis, MN 55455, USA. [7]Department of Pediatrics, Division of Rheumatology, Allergy and Immunology, University of Minnesota, Minneapolis, MN 55455, USA. [8]Division of Pediatric Hematology and Oncology, Department of Pediatrics, University of Minnesota, Minneapolis, MN 55455, USA. [9]Masonic Cancer Center, University of Minnesota, Minneapolis, MN 55455, USA. [10]Stem Cell Institute, University of Minnesota, Minneapolis, MN 55455, USA. [11]Department of Laboratory Medicine, University of California, San Francisco, San Francisco, CA 94143, USA. [12]Center for Immunology, University of Minnesota, Minneapolis, MN 55455, USA. [13]Center for Autoimmune Diseases Research, University of Minnesota, Minneapolis, MN 55455, USA.
*Corresponding author. Email: tfreedma@umn.edu
†These authors contributed equally to this work.
‡Present address: Division of Immunology and Pathogenesis, Department of Molecular and Cell Biology, University of California, Berkeley, Berkeley, CA 94170, USA.
§Present address: Department of Otolaryngology, Head and Neck Surgery, University of Minnesota, Minneapolis, MN 55455, USA.

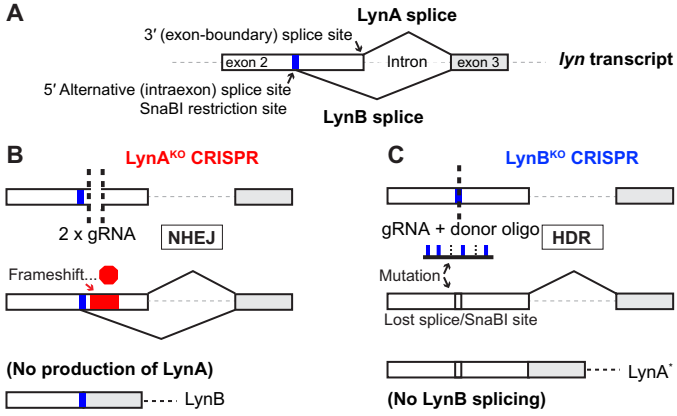

Fig. 1. Generation of LynA^{KO} and LynB^{KO} mice. (**A**) Locations of LynA and LynB splice junctions in WT *lyn* transcript; a SnaBI restriction site is situated near the LynB splice donor in exon 2. (**B**) Generating LynA^{KO} via NHEJ after double cutting within the LynA insert. (**C**) Generating LynB^{KO} via HDR from a point-mutated donor oligonucleotide template.

Lyn-deficient cells, previous studies have suggested that the roles of LynA and LynB may be distinct (*34*, *35*). Our group has observed that selective degradation of LynA results in a signaling blockade that is not reversible by activated LynB (*36*, *37*). Lack of isoform-specific knockout models, however, has remained a barrier to studying the discrete functions of LynA and LynB.

To unmask isoform-specific functions of Lyn, we used CRISPR-Cas9 gene editing to generate single-isoform LynA^{KO} and LynB^{KO} mice, each with the remaining isoform expressed at a physiological level. While LynB^{KO} mice uniformly developed a severe autoimmune disorder characterized by splenomegaly and autoantibody production, only female LynA^{KO} mice developed severe disease. Notably, either isoform of Lyn was sufficient to support B cell development, which effectively uncoupled the developmental phenotype from the skewing and expansion of myeloid and differentiated B cell populations. We found unique, isoform-specific, and sex-specific differences in subsets of myeloid cells, B cells, and T cells in the single-isoform and total Lyn^{KO} mice. Despite these differences, mice of either sex with severe splenomegaly produced autoreactive antibodies and developed lupus nephritis. These observations support a model in which LynB carries the more dominant immunosuppressive function, but LynA is uniquely required to protect against autoimmune disease in female mice.

RESULTS

Generation of LynA^{KO} and LynB^{KO} mice

We generated germline knockouts of LynA and LynB via CRISPR-Cas9 gene editing. For the LynA knockout, we injected mouse embryos with a preformed ribonucleoprotein complex (*38*, *39*) of Cas9 and two guide RNAs (gRNAs). This complex excised a short sequence near the (LynA-only) 3′ end of *Lyn* exon 2, triggering repair by nonhomologous end joining (NHEJ) (Fig. 1B). Shortened (double cut/deletion), SnaBI–sensitive (preserved 5′ splice donor), polymerase chain reaction (PCR)–screened candidates were sequenced and bred to homozygosity. The final LynA^{KO}(CRISPR) allele contained a 37-nucleotide deletion, which induced a frameshift and predicted premature termination codon at position 78 in exon 4 of the 12 LynA coding exons (fig. S1B) (*40*, *41*). Thus, the LynA splice product fit the criteria for nonsense-mediated decay (NMD) (*42*), with no alteration of the LynB splice site or mRNA sequence (fig. S1C).

For the LynB knockout, we used a single gRNA with a donor oligonucleotide as a template for homology-directed repair (HDR). The oligonucleotide contained a point mutation to ablate the LynB splice donor and a second silent mutation of the SnaBI restriction site for screening (Fig. 1C). In the final LynB^{KO}(CRISPR) allele, ablation of the LynB splice donor introduced a conservative valine-to-leucine aliphatic substitution at LynA position 24 (fig. S2).

To confirm that LynA^{V24L} was functional in LynB^{KO}, we generated F1 (LynAB^{hemi}) mice by crossing homozygous LynA^{KO}(CRISPR) and LynB^{KO}(CRISPR) parents (Fig. 2A and fig. S3A). Bone marrow–derived macrophages (BMDMs) from LynAB^{hemi} mice expressed a physiological level of LynA^{V24L} from one allele and a physiological level of LynB from the other (Fig. 2, B and C). The phenotypes of LynAB^{hemi} controls, reported throughout this paper, were indistinguishable from wild type (WT) (e.g., fig. S3B). LynA and LynA^{V24L} were equally effective initiators of signaling in an ectopic expression system (fig. S3, C and D) (*36*, *43*, *44*) and had equal susceptibility to activation-induced degradation in BMDMs (fig. S3, E and F) (*36*, *37*, *45*–*51*). We therefore considered LynA^{V24L} to be an acceptable substitute for LynA in LynB^{KO} mice. Secondarily, these controls increase our confidence that no dominant-negative LynA truncation product was expressed in LynA^{KO} mice.

Knockout of LynA and LynB, respectively, was confirmed in BMDMs from homozygous LynA^{KO}LynB$^{+/+}$ and LynB^{KO}LynA$^{+/+}$ mice (Fig. 2, A and B). Expression levels of other SFKs (Fyn, Fgr, Hck, and Src) in BMDMs were unaltered (Fig. 2B and fig. S4A). LynA expression was increased twofold in homozygous LynB^{KO}LynA$^{+/+}$ BMDMs relative to WT; we attributed this increase to LynA being the only remaining option for transcript splicing.

As the LynA CRISPR deletion was expected to trigger NMD of mature mRNA after LynA and LynB splicing, we expected to find LynB expressed at roughly physiological levels in LynA^{KO} cells. To our surprise, expression of LynB was up regulated twofold relative to WT in homozygous LynA^{KO}LynB$^{+/+}$ BMDMs (Fig. 2C). To assess whether LynB up-regulation was a feedback process triggered by cumulative loss of Lyn (A + B) or an isoform-specific regulatory effect, we generated F1 (Lyn$^{+/-}$) progeny of WT and total Lyn^{KO}(Neo) mice (*52*, *53*). Lyn$^{+/-}$ BMDMs, in which LynA and LynB are coexpressed from a single allele, had 75% reduced expression of both LynA and LynB (Fig. 2D), suggesting that maintaining a balance of LynA and LynB or a change in splicing is the dominant driver of the feedback regulation in LynA^{KO}LynB$^{+/+}$ macrophages.

We also assessed the relative expression levels of LynA and LynB in representative immune cells: DCs, macrophages, monocytes, mast cells, and B cells (Fig. 2E). Preferential expression of LynA and LynB varied by cell type, suggesting some degree of cell-specific regulation at the splicing or protein level. Splenic DCs and B cells, for example, expressed the most LynB (63 and 61% of total Lyn), whereas bone marrow–derived DCs (BMDCs) expressed the least (44% of total Lyn). Although these differences were subtle, they were consistent within each cell type and lend context to cell-specific phenotypes of LynA^{KO} and LynB^{KO} mice.

To achieve physiological expression of the remaining isoform in the LynA and LynB knockouts, we pivoted to a monoallelic expression strategy, using F1 progeny from homozygous Lyn^{KO}(Neo) × homozygous LynA^{KO}(CRISPR) or LynB^{KO}(CRISPR) parents (Fig. 2A).

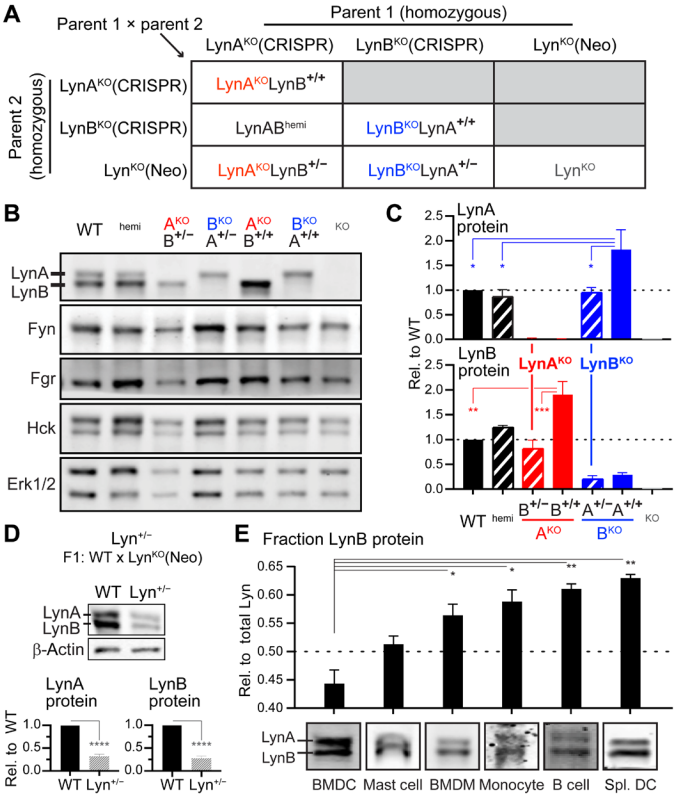

Fig. 2. SFK expression in LynA^{KO} and LynB^{KO} mice. (**A**) Breeding scheme showing parental CRISPR and neomycin (Neo) (*53*) knockouts. LynA^{KO}LynB$^{+/+}$ progeny have biallelic expression of LynB, whereas LynA^{KO}LynB$^{+/−}$ have monoallelic expression of LynB; allelic expression is reversed in the LynB^{KO} series. (**B**) Immunoblot showing SFK expression in WT, (LynAB)^{hemi}, (Lyn)A^{KO}, (Lyn)B^{KO}, and (total Lyn)^{KO} BMDMs; Erk1/2 shows protein loading. (**C**) Quantification of LynA and LynB protein in BMDMs from male and female mice, corrected for total protein staining (*74*) and background in Lyn^{KO}, reported relative to WT. Residual LynB signal in LynB^{KO} was caused by LynA bleed-through. Error bars are SEM from at least three independent experiments ($n = 3$ to 5). Unless otherwise specified, significance: one-way ANOVA with Tukey's multiple comparisons test, ****$P < 0.0001$, ***$P < 0.002$, **$P < 0.01$, and *$P < 0.05$. Not annotated: In the Lyn(B or A) quantifications, [WT/LynAB^{hemi}] versus [Lyn(A or B)^{KO}/Lyn^{KO}] pairs were significantly different. Other pairs were not significant. WT and Csk^{AS} BMDMs were both used in this analysis. (**D**) Total Lyn protein expression in WT and Lyn$^{+/−}$ BMDMs, corrected as above; in this and other figures, β-actin shows protein loading. Significance: unpaired *t* test; error bars: SEM ($n = 4$). (**E**) Relative LynB protein content in immune cells, with representative immunoblot images for BMDCs, bone marrow–derived mast cells, BMDMs, peripheral blood monocytes, splenic B cells, and splenic DCs (Spl. DC). Error bars: SEM ($n = 3$ to 13).

BMDMs from LynA^{KO}LynB$^{+/−}$ and LynB^{KO}LynA$^{+/−}$ mice expressed the remaining Lyn isoform at levels comparable to WT (Fig. 2, B and C). Single-isoform expression did not systematically affect the levels of other SFKs in BMDMs and BMDCs (Fig. 2B, fig. S4, A and B) and did not impair IFN-γ–dependent up-regulation of Lyn expression (fig. S5) (*37*)). LynA^{KO}LynB$^{+/−}$ and LynB^{KO}LynA$^{+/−}$ mice are hereafter referred to as "LynA^{KO}" and "LynB^{KO}," respectively (Fig. 2C).

Severe splenomegaly in aging LynB^{KO} mice and female LynA^{KO} mice

Like Lyn^{KO} mice (*4*, *17*, *18*), male and female LynB^{KO} mice developed mild-to-severe splenomegaly between 5 and 8.5 months of age (Fig. 3 and fig. S6A). In contrast, only female LynA^{KO} mice developed severe splenomegaly. The effects of LynA and LynB knockout were not additive, with the most severely affected single-isoform knockouts comparable in spleen mass to total Lyn^{KO}. These data suggest that LynB performs the dominant regulatory function for both sexes, while LynA is uniquely required for maintaining normal cell numbers in the spleens of female mice. This observation did not extend to body mass, another typical indicator of disease, in part due to high variability in WT female mice (fig. S6B). Moreover, as Lyn and Lyn-expressing myeloid cells regulate adipose, bone, and other tissues (*54*, *55*), interpretation of differences in body mass is not straightforward.

Unique myeloid cell profiles in LynA^{KO} and LynB^{KO} mice

Because splenomegaly in total Lyn^{KO} mice stems from myeloproliferation, especially in monocyte and granulocyte (neutrophil + eosinophil) populations (*11*, *32*, *56*), we used flow cytometry to quantify splenic myeloid cells (fig. S7). With the exception of an early increase in patrolling monocytes in total Lyn^{KO} mice (*57*), myeloid cell expansion developed between 5 months (fig. S8) and 8.5 months of age.

Spleens from aged Lyn^{KO}, LynB^{KO}, and female LynA^{KO} mice had distinctive myeloid cell imbalances. Most notably, the cDC2 (conventional type 2 DC) pool was increased in LynA^{KO} and LynB^{KO} mice but not in total Lyn^{KO} mice (Fig. 4A and fig. S9). Only spleens from female single-isoform mice had a secondary expansion of monocytes within the myeloid cell pool (Fig. 4B and fig. S10). Neither LynA^{KO} nor LynB^{KO} spleens had the granulocyte expansion characteristic of the total Lyn^{KO} (Fig. 4C and fig. S11) (*11*, *32*, *56*).

The monocyte expansion phenotype in LynA^{KO} and LynB^{KO} mice was milder and more sexually dimorphic than in total Lyn^{KO} mice. Phenotypes in the female single-isoform knockouts varied in severity from mild (elevated total monocyte fraction) in female LynA^{KO} spleens to moderate (elevated patrolling monocyte numbers) in female LynB^{KO} spleens to severe (elevated classical, intermediate, and/or patrolling monocyte numbers) in male and female Lyn^{KO} spleens.

The DC expansion phenotype was present in male and female LynA^{KO} and LynB^{KO} mice. cDC1 numbers were not affected in any of the Lyn knockouts, but cDC2 and other DC populations were increased in LynA^{KO} and LynB^{KO} mice. Phenotypes varied in severity from mild (elevated cDC2:cDC1 ratio) in LynA^{KO} spleens to severe (elevated cDC2 numbers) in LynB^{KO} spleens.

A population of CD64$^{−}$CD11c^{+}SiglecF$^{−}$ cells was also increased in LynB^{KO} but not total Lyn^{KO} spleens. On the basis of their low expression of major histocompatibility complex class II (MHCII) and lack of B cell markers, we tentatively classified these cells as pre-DCs (fig. S7) (*58*–*60*). In all the Lyn knockouts, this putative pre-DC population up-regulated CD80/86, which was absent or expressed at low levels in WT pre-DCs (fig. S7, inset) (*60*).

Together, the unique expansion of DCs in the single-isoform knockouts and additional monocyte expansion in the female mice created a continuum of myeloid dysregulation, ranging from the mildest phenotype for male LynA^{KO} spleens to more severe phenotypes in LynB^{KO} and female LynA^{KO} spleens (Fig. 4D). Severe phenotypes in male and female mice indicate a dominant role for LynB in maintaining splenic myeloid populations. Loss of both isoforms in the total Lyn knockout restored a WT-like balance of DCs but caused the most severe monocyte and granulocyte expansion.

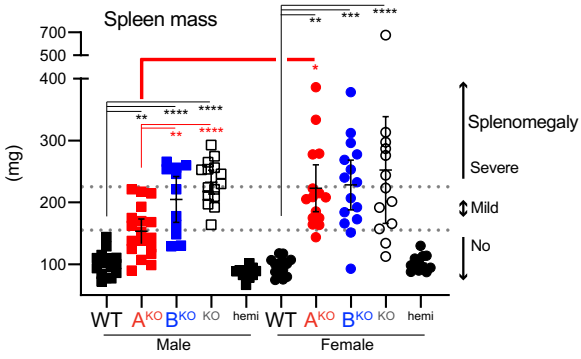

Fig. 3. LynB^{KO} mice and female LynA^{KO} mice develop severe splenomegaly. Spleen masses from four to six different cohorts of male mice aged 8.5 ± 0.4 months and female mice aged 8.4 ± 0.2 months; error bars: 95% CIs. In this and other figures, in addition to the annotated comparisons (asterisks colored by genotype), there were no significant differences between LynAB^{hemi} and WT. Dotted lines reflect phenotypic scoring: no splenomegaly (spleen <155 mg), mild splenomegaly (155 to 225 mg), or severe splenomegaly (>225 mg), referenced in later figures.

Myeloid cells from Lyn^{KO} mice are more proinflammatory and activated than cells from single-isoform knockouts

Most myeloid cell populations in spleens from Lyn^{KO} mice expressed higher levels of proinflammatory and activation-associated markers than cells from either of the single-isoform knockouts, suggesting a more severe inflammatory phenotype. Female LynA^{KO} and LynB^{KO} mice, however, had increased expression of proinflammatory markers compared to WT. Splenic macrophages from female LynA^{KO} and LynB^{KO} mice had some elevation of CD80/86 and a significant increase in CD11c, comparable to Lyn^{KO} (Fig. 5A). Male LynA^{KO} and male LynB^{KO} macrophages were not significantly different from WT. This sex-specific effect was absent in the total Lyn^{KO}. For other markers that were responsive to Lyn expression, including CD11b expression on neutrophils, MHCII on cDC2s, and CD80/86 on pDCs, Lyn^{KO} cells consistently had the most severe phenotype (Fig. 5B and fig. S12).

In alignment with their preferential expression of hyperstimulatory markers on cDC2 and pDC populations (*32*, *61*) and CD11b^{hi}/expanded neutrophils (*62*, *63*), only total Lyn^{KO} mice had significantly elevated serum levels of the proinflammatory cytokine BAFF (Fig. 5C). The trend toward milder elevation of serum BAFF in LynA^{KO} and LynB^{KO} mice also paralleled the trend toward more modest expression levels of MHCII and CD80/86 on cDC2 and pDC subsets.

From these data, we conclude that loss of both Lyn isoforms causes more severe inflammatory dysregulation of myeloid cells than loss of either isoform alone. Notably, costimulatory markers are also most profoundly dysregulated on DCs in the total Lyn^{KO}, despite the greater effect of isoform-specific LynA or LynB knockout on DC numbers. This could also suggest that granulocytes, not DCs, are the major drivers of BAFF production (*64*).

LynA or LynB expression is sufficient to restore B cell development

Reduced B cell numbers, attributed to cell death during progression through transitional stages 1 to 3 of development (*56*), are a hallmark of immune dysregulation in Lyn^{KO} mice (*17*). Expression of either LynA or LynB, however, was sufficient to rescue B cell numbers to near-WT levels in male and female mice (Fig. 6A). Spleens from 8.5-month-old LynA^{KO} and LynB^{KO} mice had significantly more T2 and T3 B cells than those from Lyn^{KO} mice (Fig. 6, B and C, and fig. S13), which appeared relatively enriched in T1 cells due to cell loss at later stages (fig. S14) (*65*, *66*). LynA^{KO} and LynB^{KO} transitional cells generally had intermediate levels of MHCII expression, between WT and the significantly elevated levels in total Lyn^{KO} cells (Fig. 6D) (*32*).

LynA^{KO} and LynB^{KO} spleens also contained more follicular (Fo) and marginal zone (MZ) B cells than those of total Lyn^{KO} (Fig. 6E and fig. S14), and these cells had levels of surface MHCII comparable to WT (Fig. 6F) (*32*, *67*, *68*). LynA or LynB expression also restored normal immunoglobulin M (IgM) expression within the Fo B cell population (fig. S14).

Together, either LynA or LynB expression appears sufficient to restore B cell development, supporting production of MZ and Fo B cell populations in WT-like numbers. However, these populations do not experience any further increase in proportion to splenomegaly. Increased surface MHCII could reflect elevated BCR signaling in early transitional populations of LynA^{KO} and LynB^{KO} B cells (*69*), but differentiated MZ and Fo B cell populations do not appear to be hyperresponsive. Thus, deletion of either isoform of Lyn effectively uncouples the B cell development defect from the other myeloid and B cell drivers of autoimmunity observed in total Lyn^{KO} mice.

Enrichment of differentiated B cells in spleens from single-isoform Lyn knockout mice

Activated and autoreactive populations of differentiated B cells are enriched in total Lyn^{KO} mice (*56*, *70*), and we performed flow cytometry to quantify these populations in the single-isoform knockouts (fig. S13). Expansion of differentiated B cell pools in the Lyn knockouts occurred between 5 months (fig. S15) and 8.5 months of age. In the single-isoform knockouts but not the total Lyn^{KO}, GL7^{+} germinal center (GC) or activated B cells, B1 cells, and a CD19^{hi}CD21/35^{-} population likely comprising ABCs increased roughly in proportion to spleen size (Fig. 7A and fig. S16A). In contrast, plasmablasts and plasma cells, including the IgM^{+} unswitched population reported to drive the plasma cell expansion in Lyn^{KO} spleens (fig. S13, inset) (*71*), were not significantly more numerous in LynA^{KO} or LynB^{KO} than in Lyn^{KO} (Fig. 7B). Immunoglobulin class-switched B cells, like Fo and MZ B cells, were not significantly expanded in the single-isoform knockouts relative to WT (fig. S16A). Overall, these expansion profiles resulted in a relative enrichment of GL7^{+} cells, B1 cells, and ABCs within the total B cell population in LynA^{KO}, LynB^{KO}, and Lyn^{KO}. Only Lyn^{KO} spleens, however, were significantly enriched in IgM^{+} plasmablasts and plasma cells and switched B cells (fig. S16B) (*32*, *52*).

GL7^{+} B cells were elevated in both male and female LynA^{KO} mice, although females trended toward a more severe phenotype (fig. S17). In total Lyn^{KO} mice, the increased fractional content of activated B cell subsets was largely attributable to the profound loss of Fo and MZ B cells (Fig. 7C). Overall, GL7^{+} B cells, B1 B cells, and ABCs increased 5- to 10-fold, roughly in proportion to spleen mass in LynA^{KO} and LynB^{KO} mice, whereas plasma and switched B cells failed to expand similarly (Fig. 7D).

Analysis of T cell subsets, which lack Lyn expression but respond to changes in myeloid and B cell activation, revealed additional differences in the single-isoform knockout mice (fig. S18). Although CD4^{+} and CD8^{+} populations of T cells were expanded in LynA^{KO} and LynB^{KO} spleens relative to total Lyn^{KO}, natural killer (NK) cells and most T cell subsets had few significant differences (fig. S19).

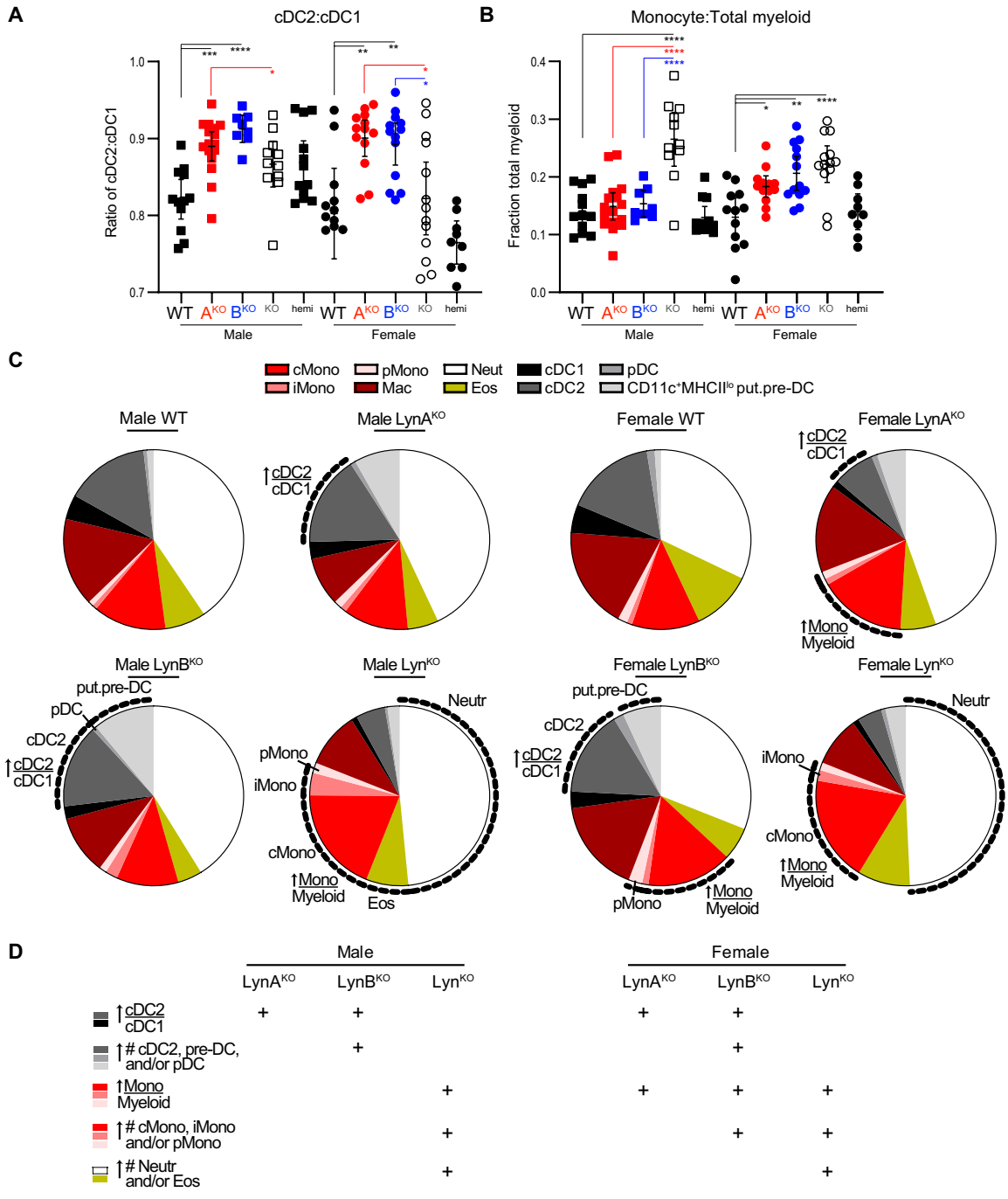

Fig. 4. Isoform- and sex-specific differences in splenic monocyte and DC composition of LynA^{KO} and LynB^{KO} mice. Spleen cell suspensions from 8.5-month-old mice were stained for myeloid cell markers and analyzed by flow cytometry. Counting beads were used to calculate the total number of cells per spleen, from which the fractional content of each cell type was calculated. Populations: Classical monocyte (cMono: CD64^{+}MerTK^{-}Ly6C^{hi}), intermediate monocyte (iMono: Ly6C^{intermediate}), patrolling monocyte (pMono: Ly6C^{lo}), macrophage (Mac: CD64^{+}MerTK^{+}), conventional type 1 DC (cDC1: CD64^{-}CD11c^{hi}MHCII^{hi}CD11b^{lo}XCR1^{hi}), conventional type 2 DC (cDC2: CD11b^{hi}XCR1^{lo}), CD11c^{+}SiglecF^{-}MHCII^{lo} putative pre-DC [put.pre-DC (*58*–*60*)], plasmacytoid DC (pDC: CD11c^{lo}Ly6C^{hi}PDCA1^{hi}), eosinophil (Eos: Ly6G^{med}Siglec-F^{+}SSC^{hi}), and neutrophil (Neut: Ly6G^{hi}). (**A** and **B**) Fractional content of splenic monocyte (A) and cDC2 (B) populations. Error bars: 95% CI. Asterisks are statistical comparisons colored by genotype; no significant differences between LynAB^{hemi} and WT populations. Data pooled from four to six separate cohort analyses. Gating is shown in fig. S7, and cell counts and statistics are shown in figs. S9 to S11. (**C**) Myeloid cell populations in Lyn knockout mice. Labels and dotted lines highlight total splenic cell populations (or fractional populations, where indicated) that were increased significantly relative to same-sex WT comparators. LynAB^{hemi} analyses are included in the supplement. (**D**) Summary of myeloid cell imbalances in Lyn knockout mice.

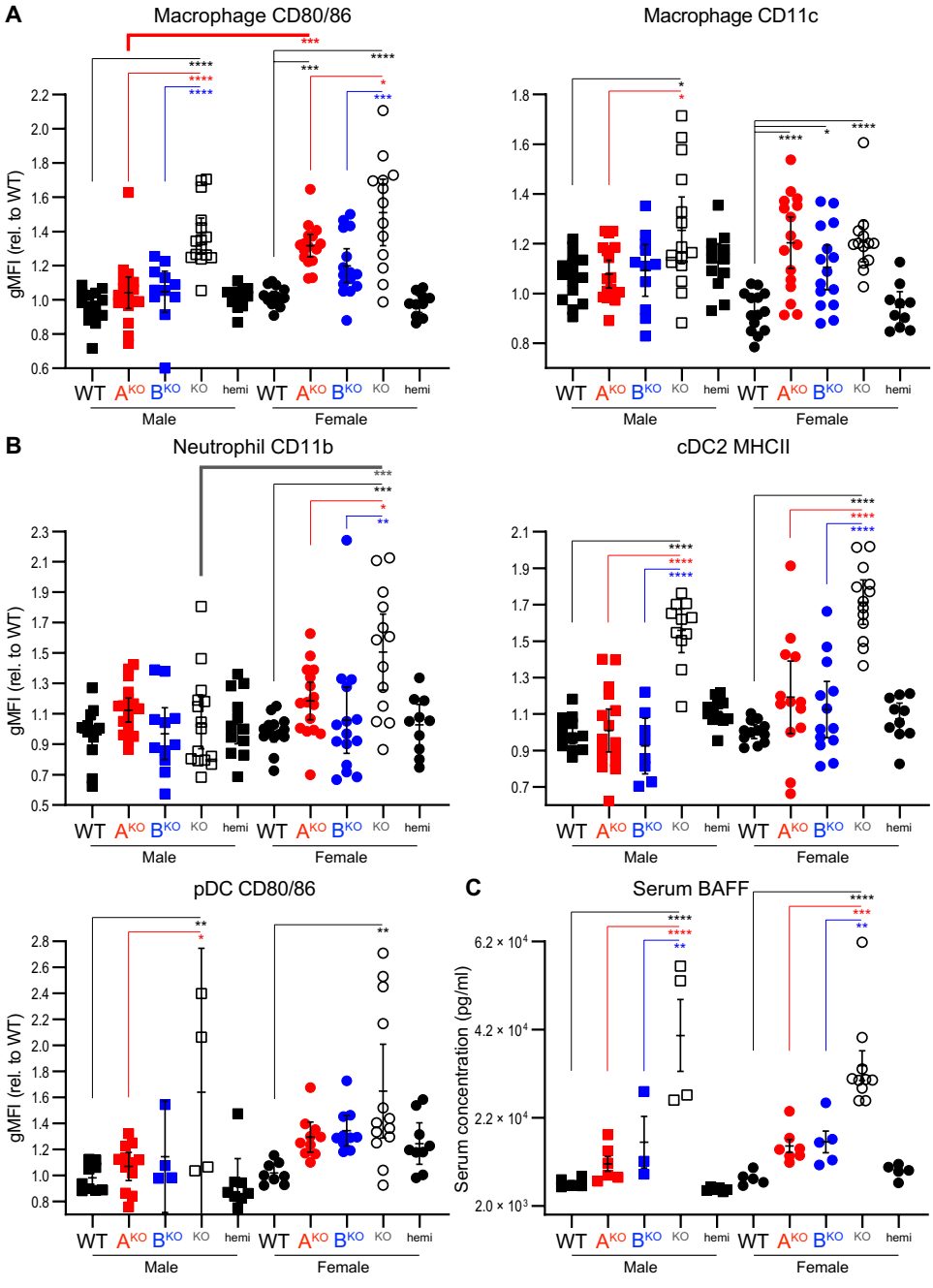

Fig. 5. Differential polarization of myeloid cells and BAFF production from male and female LynA^{KO} and LynB^{KO} mice. Spleen cell suspensions from 8.5-month-old male and female mice were stained for markers of myeloid polarization and analyzed by flow cytometry. Geometric mean fluorescence intensities (gMFIs) reported relative to the average WT value for each cell type and marker within each of four to six experiment days. Statistical annotations and error bars as described in Fig. 4. (**A**) Expression of proinflammatory polarization markers by MerTK^{+} macrophages. (**B**) Expression of neutrophil and DC activation/polarization markers. (**C**) Serum from 8.5-month-old male and female mice was assayed for BAFF using ELISA; error bars: SEM.

In summary, despite supporting relatively normal B cell development and (cell extrinsically) T cell development, expression of either LynA or LynB alone was not sufficient to limit the production of activated and autoimmunity-driving B cells. This unique constellation of lymphocyte effects in LynA^{KO} and LynB^{KO} mice effectively uncoupled the B cell developmental phenotype from dysregulation of mature and further differentiated subsets.

LynA^{KO} and LynB^{KO} mice with severe splenomegaly develop autoimmune disease

Total Lyn^{KO} mice develop renal inflammation triggered by ANA and complement deposition. Kidneys from LynA^{KO} and LynB^{KO} mice with splenomegaly also had immune cell infiltration, evidence of glomerular and tubular inflammation (Fig. 8, A and B), deposition of IgG and complement (C3) (Fig. 8, C and D), and fibrosis

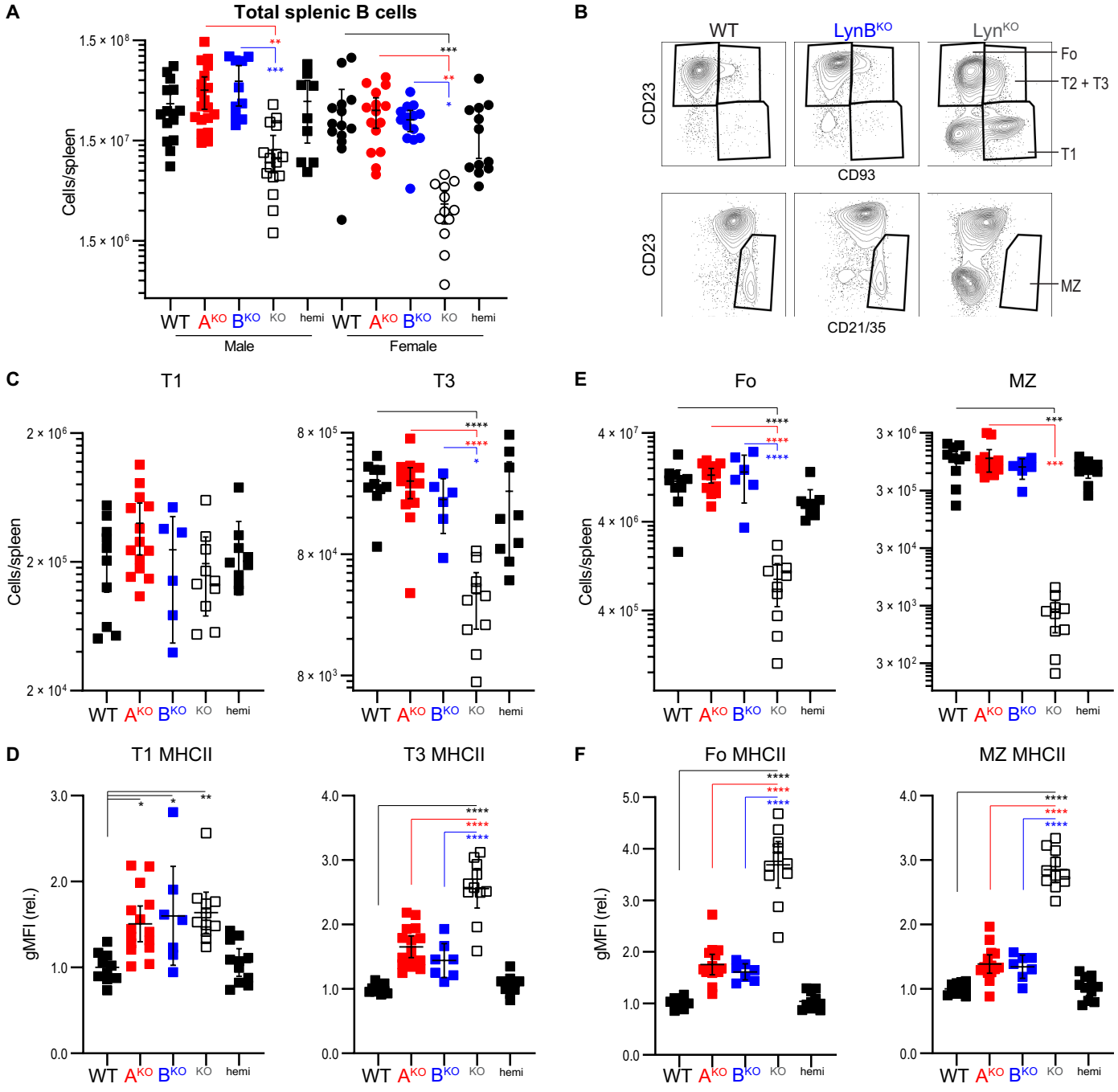

Fig. 6. B cell development is rescued by expression of LynA or LynB. Spleen cell suspensions from 8.5-month-old male and female mice were stained for markers of B cell development and analyzed by flow cytometry on four to six cohort/experiment days. (**A**) Total spleen B cell numbers; error bars: 95% CI. (**B**) Representative flow cytometry plots showing gates for follicular B cells (Fo: $CD93^{-}CD23^{+}$), T1 B cells ($CD93^{+}CD23^{-}$), T2/T3 B cells ($CD93^{+}CD23^{+}$), and marginal zone B cells (MZ: $CD23^{-}CD21/35^{+}$). (**C**) Total numbers of B cell transitional populations T1 and IgM^{lo} T3 per spleen. (**D**) Surface MHCII expression on T1 and T3 B cells relative to WT within each experiment. (**E**) Total numbers of Fo and MZ B cells per spleen. (**F**) Surface MHCII expression on Fo and MZ B cells.

(Fig. 8, E and F). The levels of renal IgG, C3, and trichrome staining were comparable in all the Lyn knockout genotypes, coinciding roughly with the splenomegaly profile. This suggests that loss of either LynA or LynB is sufficient to drive autoimmunity in mice with severely dysregulated myeloid and B cell populations, mostly $LynB^{KO}$ mice and female $LynA^{KO}$ mice. This also indicates that the blockade in B cell development in total Lyn^{KO} mice is not a necessary precursor to the later dysregulation of differentiated B cells that drives autoimmunity.

ANA production (Fig. 9A) was assayed using sera from $LynA^{KO}$ and $LynB^{KO}$ mice. As with C3/IgG deposition in the kidney, the frequency of serum ANA positivity mirrored the pattern of splenomegaly

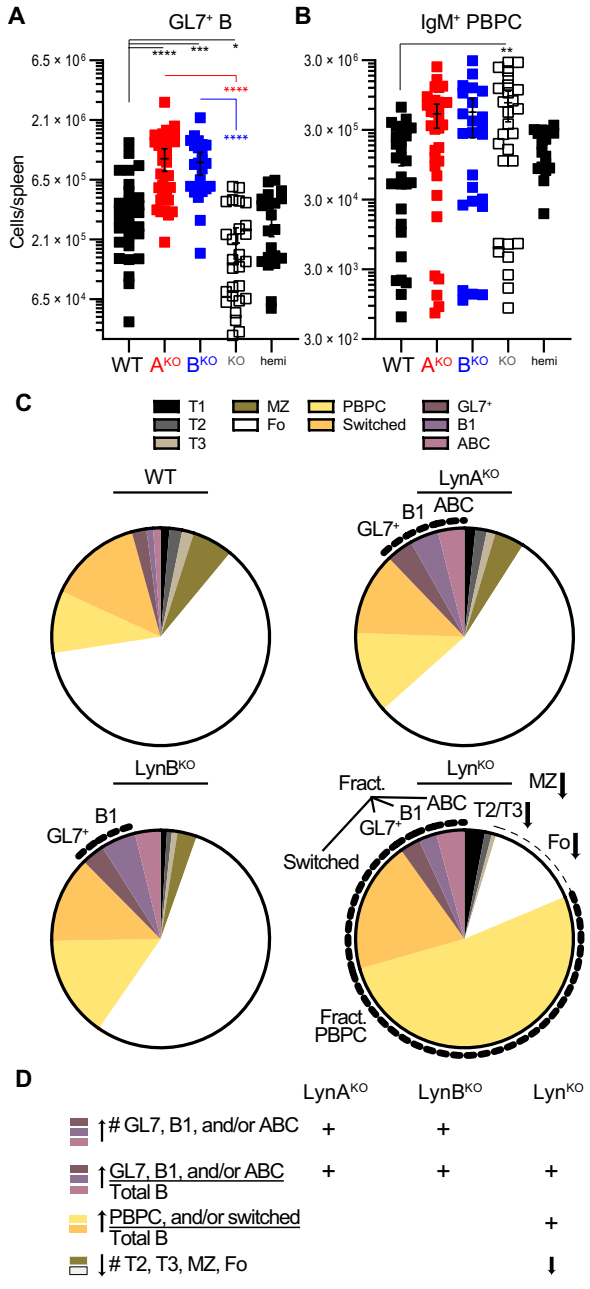

Fig. 7. Unique expansion of activated and autoimmunity-associated B cell subsets in LynA^{KO} and LynB^{KO} mice. Spleen cell suspensions from 8.5-month-old male and female mice were stained for B cell markers and analyzed by flow cytometry. Populations of differentiated B cells: GL7$^+$ GC and activated B cells (GL7$^+$: B220$^+$GL7^{hi}), B1 B cells (B220$^+$CD11b^{hi}), ABCs (CD19^{hi}CD21/35$^-$), plasma cells and plasmablasts (PBPC: CD138^{hi}IgH+L^{hi}), and switched B cells (IgM$^-$IgD$^-$). (**A**) Total splenic numbers of GL7$^+$ B cells. (**B**) Total splenic numbers of IgM$^+$ (unswitched) plasma cells and plasmablasts. (**C**) Fractional content of each B cell subset within the total B cell population; the PBPC pool includes IgM$^+$ and IgM$^-$ cells. Labels and dotted lines highlight total splenic cell populations (or fractional populations, where indicated) that differ significantly from WT comparators. Gating is shown in fig. S13, and raw cell counts, statistics, and LynAB^{hemi} data are shown in Fig. 6 and figs. S14 and S16. No significant differences between LynAB^{hemi} and WT. Data pooled from four to six separate cohort analyses. (**D**) Summary of Lyn knockout splenic B cell composition.

within each genotype (Fig. 9B). In a mixed-sex analysis, LynB^{KO} sera were primarily ANA positive, whereas LynA^{KO} sera were more heterogeneous.

IgM levels were highest in sera from total Lyn^{KO} mice, roughly doubling the intermediate phenotypes of the single-isoform knockouts (Fig. 9C) and mirroring the pattern of BAFF production and the expansion of IgM$^+$ plasmablasts and plasma cells. Nevertheless, IgM levels in LynA^{KO} and LynB^{KO} sera were still elevated relative to WT, with loss of both Lyn isoforms trending toward an additive effect.

Last, we performed immunofluorescence microscopy on frozen spleen sections from 8.5-month-old mice with varying degrees of splenomegaly, using protein markers expressed by B cells (B220), GC/activated B cells (GL7), myeloid cells (CD11b), and T cells [T cell receptor β (TCRβ)] (Fig. 10A and figs. S20 and S21). Disruption of spleen architecture agreed with other indicators of disease, including splenomegaly. Focusing on lymphoid follicle organization (*72*) via immunofluorescence (Fig. 10B) or hematoxylin and eosin (H&E) staining (Fig. 10C) revealed a series of intermediate phenotypes: WT and LynA^{KO} mice with no or mild disease had well-formed B cell follicles, GCs, and T cell zones. LynB^{KO} and Lyn^{KO} mice with moderate-to-severe disease displayed follicular effacement with diffuse GCs and follicles. Together, these data suggest that severe disease is accompanied by disruptions in spleen architecture.

DISCUSSION

Dissecting the contributions of the two Lyn isoforms has been stymied by a lack of experimental tools. LynB has no unique sequence, making the development of LynB-specific antibodies and RNA silencing reagents infeasible. In addition, LynB is produced from an intra-exon splice site, rendering traditional knockout and recombination/excision approaches intractable. We pioneered two CRISPR-Cas9 strategies to create splice-fixed LynB-only or LynA-only mouse strains: For LynA^{KO}, we engineered a deletion and frameshift in the unique LynA insert, and for LynB^{KO}, we ablated the LynB splice donor site. These new models can be used as hemizygotes or homozygotes for physiological or supraphysiological expression of the remaining isoform. We have found that LynB has the dominant regulatory role in mice of both sexes, but that LynA expression is uniquely required to prevent autoimmunity in female mice. Our data suggest that myeloid cells and B cells have different requirements for LynA and LynB expression, and the two isoforms are differentially required for development, proliferation, and reactivity. Last, we report that the relative expression levels of LynA and LynB are controlled by feedback regulation and maintained in a cell-specific manner.

We do not yet know why female mice are more reliant on LynA expression for immune homeostasis. It is possible that an added level of immune restraint is necessary simply because females are generally more prone to inflammation and thus easier to propel toward autoimmunity. It is also possible that LynA, and perhaps also LynB, has a direct function in hormone signaling, TLR7 signaling, or other sexually dimorphic signaling pathways. In our colony, female LynA^{KO} mice (and by some criteria female LynB^{KO} mice) had greater proinflammatory polarization of macrophages and with GL7$^+$ B cells expanding proportionally with increased spleen size. When LynA^{KO} mice did develop disease, the accompanying splenomegaly and glomerulonephritis were comparable to LynB^{KO} and Lyn^{KO} phenotypes, suggesting that the degree of disease could not be explained simply by the relative loss of Lyn expression in each genotype. Future studies will

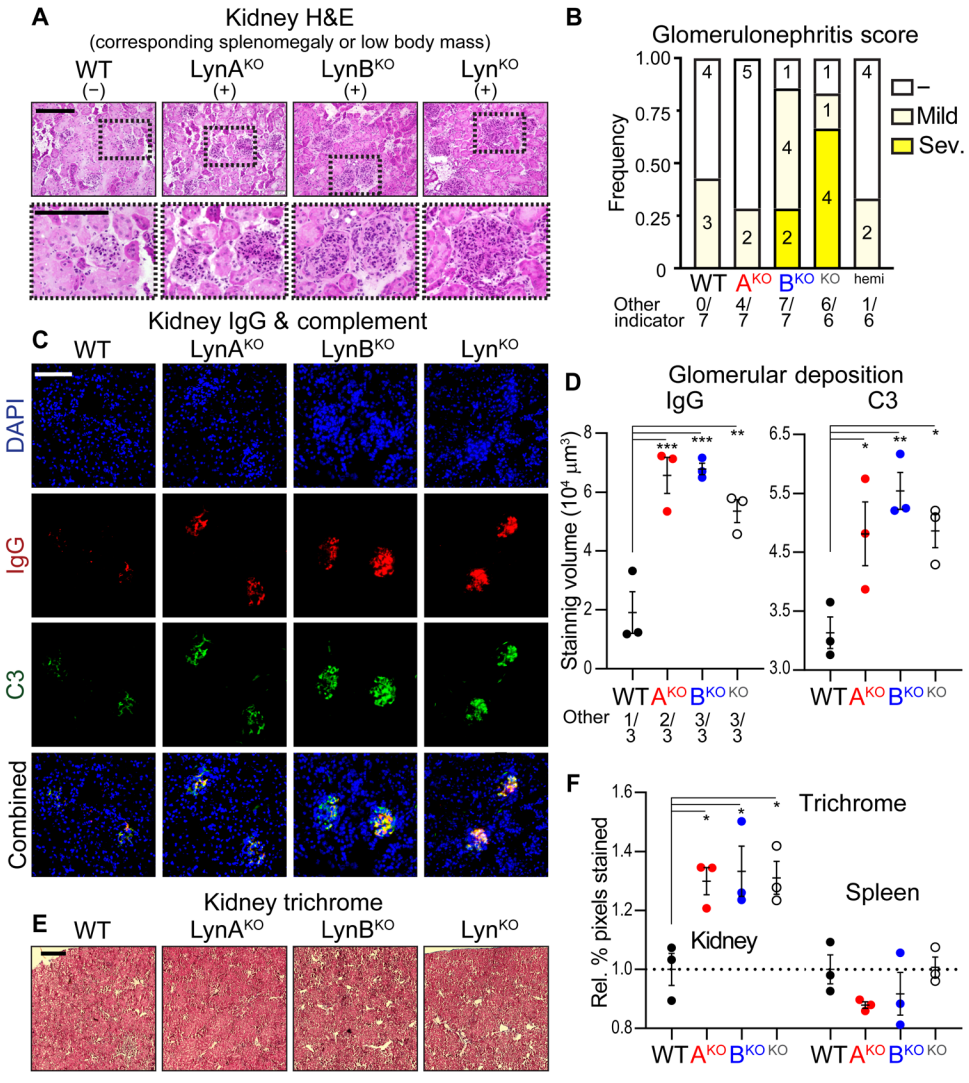

Fig. 8. LynA^{KO} and LynB^{KO} mice with splenomegaly or low body mass develop autoimmune disease. Mice (8.5 months old) were tested for indicators of autoimmunity and lupus nephritis. (**A** to **D**) Kidney and spleen sections and epifluorescence images were obtained from female and male mice with varying degrees of splenomegaly and body mass. (A) Representative hematoxylin and eosin (H&E)–stained kidney sections were deidentified and scored for glomerulonephritis; scale bar, 200 µm. Boxed regions are enlarged in the bottom row. Occurrence of splenomegaly or low body mass in the same individual (+ yes, – no), referenced after unblinding as defined in Fig. 3. Other indicators of disease are similar in all image panels. (B) Frequency of no (–), mild, or severe (Sev.) glomerulonephritis in clinical scoring; numbers reflect scores from sections prepared from individual mice; corresponding frequencies of splenomegaly and low body mass are indicated. Analysis pool: WT 5 M + 2 F, LynA^{KO} 4 M + 3 F, LynB^{KO} 2 M + 5 F, Lyn^{KO} 5 M + 1 F, LynAB^{hemi} 1 M + 5 F. (C) Immunofluorescence microscopy images showing nuclei (DAPI), IgG deposition (Texas Red), and C3 deposition (FITC), $n = 3$; scale bar, 100 µm. Analysis pool for (C) to (F): WT 1 M + 2 F, LynA^{KO} 3 F, LynB^{KO} 3 F, Lyn^{KO} 3 M, and LynAB^{hemi} 1 M + 2 F. (D) Quantification of IgG and C3 staining, using Imaris software; error bars, SEM. Corresponding frequencies of splenomegaly or low body mass are indicated; the same individuals were used for all other quantifications in this figure. (**E**) Masson's trichrome (collagen, fibrin, and erythrocyte) staining of kidney; scale bar, 500 µm. (**F**) Quantification of trichrome staining in kidney and spleen. NIH ImageJ software was used to deconvolute and perform region-of-interest analysis; error bars, SEM.

investigate dose- and pathway-specific mechanisms underlying these differences.

More generally, splenocyte expansion in the single-isoform knockouts was dominated by parallel increases in differentiated GL7$^+$ B cell, B1, and ABC populations and by some DC subsets; monocyte numbers were additionally expanded in female LynA^{KO} and LynB^{KO} mice. In contrast, splenomegaly in both male and female Lyn^{KO} mice was predominantly driven by granulocyte and monocyte expansion. With the exception of IgM$^+$ plasmablasts/plasma cells, imbalances in B cell populations generally owed more to a paucity of MZ and Fo B cells than to proliferation of autoreactive subsets. These data suggest that expression of either LynA or LynB is sufficient to restore B cell development and promote increases in GL7$^+$ and other B cell populations in parallel with myeloid cell expansion. Expression of either LynA or LynB is only partially able to rescue the bias toward IgM-producing plasma cells seen in Lyn^{KO} mice. This differential requirement for Lyn expression in developing and differentiated cell subsets could stem from differential functions of LynA and LynB in the more mature cell types or the greater reliance on catalytic BCR signaling function during B cell development versus

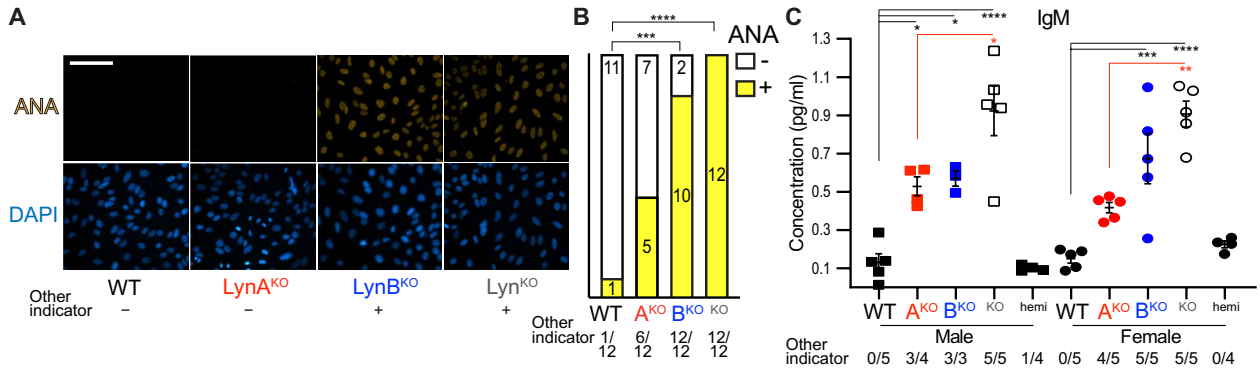

Fig. 9. LynA^{KO} and LynB^{KO} mice with splenomegaly or low body mass produce ANA and have elevated levels of serum IgM. Serum was collected from 8.5-month-old male and female mice and assayed for antibody production. (**A**) Serum ANA detection via FITC staining of Hep-2 cells. Occurrence of splenomegaly or low body mass in the same individual is indicated (+ yes, – no). (**B**) Frequency of ANA negativity (–) and positivity (+). Occurrence of splenomegaly or low body mass in the same individual (+ yes, – no) as defined in Fig. 3. Significance for raw contingency data was assessed via two-sided Fisher's exact test with Bonferroni correction for multiple comparisons. Analysis pool: WT 4 M + 8 F, LynA^{KO} 6 M + 6 F, LynB^{KO} 4 M + 8 F, and Lyn^{KO} 6 M + 6 F. (**C**) ELISA-derived IgM levels and associated splenomegaly or low body mass; error bars, SEM.

more stoichiometric adaptor functions in differentiated B and myeloid cells.

Clear phenotypic differences between Lyn$^{+/-}$ (*52*), LynA^{KO}, and LynB^{KO} mice could also support a model for some distinct functions of LynA and LynB, but with caveats. Although these comparison studies were performed on the same C57BL/6 strain background, colony-to-colony variation could influence disease kinetics and severity. In addition, we cannot make absolute comparisons of LynA and LynB protein concentrations across genotypes in vivo. Total expression of Lyn (A + B) is regulated by cell type and inflammatory environment (*36*, *37*), and we have found subtle but consistent differences in the LynA:LynB ratio in different cell types. Nevertheless, from BMDMs, we estimate that LynA^{KO} mice lose 45% of total Lyn, LynB^{KO} mice lose 55%, and Lyn$^{+/-}$ mice lose 75%. Despite a more severe presumed Lyn deficiency, Lyn$^{+/-}$ mice were reported to develop less severe glomerulonephritis and less severe MZ/T2 B cell deficits (*17*, *52*, *67*) than observed in our single-isoform knockout mice. It could be that loss of a single Lyn isoform is more devastating than a balanced 75% depletion of LynA and LynB, and this should be the subject of future studies. In addition, the loss of either LynA or LynB alone produces an enrichment of DCs not found in the total knockout, suggesting that balanced expression of both isoforms is required for homeostatic control of DC populations.

LynB generally appears to be the dominant immunosuppressive isoform, with LynB deletion causing severe autoimmune disease in male and female mice. For some indicators (splenomegaly, glomerular IgG and C3 deposition, and kidney fibrosis), LynB^{KO} and total Lyn^{KO} mice developed equally severe phenotypes. In other cases (serum IgM and BAFF, glomerular immune infiltration, myeloid cell polarization, and monocyte/granulocyte expansion), LynB^{KO} mice had less severe phenotypes than total Lyn^{KO} mice, suggesting an additive effect with LynA. LynA and LynB seemed equally capable of promoting B cell development, regulating myeloid cell polarization and restraining myeloid-driven inflammation. Given the increased number of activated/inflammatory B cell types in LynA^{KO} and LynB^{KO} mice, future studies will be aimed at determining whether the single-isoform knockouts have a more B cell–initiated than myeloid cell–initiated form of autoimmune disease. Our data suggest that LynA^{KO} and LynB^{KO} manifestations of autoimmune disease are mechanistically distinct, given their peculiar myeloid cell expansion profiles and apparent restoration of BCR-dependent development.

Last, the up regulation of LynA protein in the homozygous LynB^{KO} could be evidence of a feedback mechanism sensing LynA:LynB balance in cells. This is not a dose sensor for total Lyn, as Lyn$^{+/-}$ cells have no compensatory changes in expression. Lyn-specific feedback, independent of other SFKs, would reinforce the unique importance of balancing activating and inhibitory functions of Lyn. Our observation of cell type–specific LynA:LynB ratios further supports the idea that LynA and LynB levels are sensed and regulated. This process could be mediated by splicing factors, as in epithelial and cancer cells (*35*), or, as in mast cells and macrophages, by regulating the expression of the E3 ubiquitin ligase c-Cbl, which preferentially targets LynA for degradation (*36*, *37*). Future studies will focus on these different contributions.

In summary, we have generated two new models of SLE, in which myeloid cell dysregulation and accumulation of activated B cells are offset by relatively normal B cell development and myeloid cell polarization. Selective expression of LynA or LynB is cell-specific and reveals a sexual dimorphism in the requirement for LynA expression to prevent autoimmune disease in female mice. As no sex-specific effects have been reported in Lyn^{KO} mice, the more subtle and female-specific LynA^{KO} disease is an opportunity to explore sexual dimorphism and cell-specific mechanisms of lupus progression. Definition of overlapping versus isoform-specific regulatory modes will inspire new ways of manipulating these signaling processes to restore immune balance in patients with SLE and other autoimmune diseases.

MATERIALS AND METHODS

Mouse strains and housing

All animal use complied with University of Minnesota/American Association for Accreditation of Laboratory Animal Care and National Institutes of Health (NIH) policy, under Animal Welfare Assurance number A3456-01 and Institutional Animal Care and Use Committee protocol no. 1910-37487A. Animals were housed in a specific pathogen–free facility under the supervision of a licensed

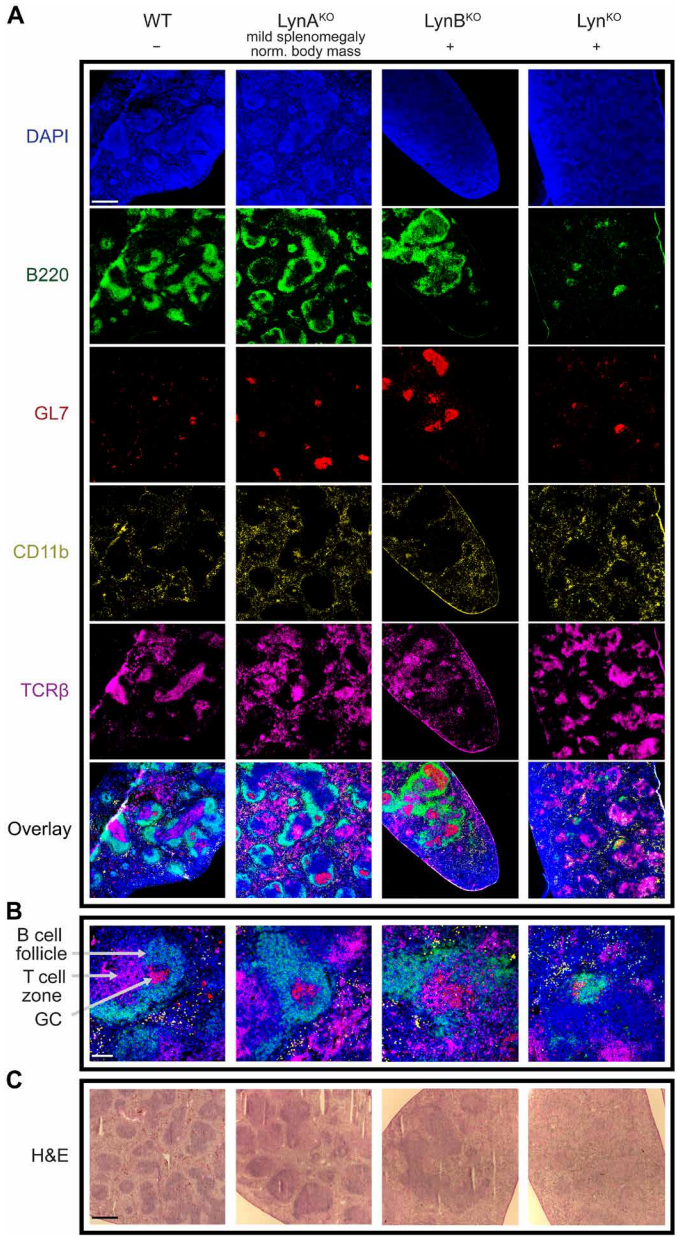

Fig. 10. Splenomegaly in male LynA^{KO} and LynB^{KO} mice corresponds with disruptions in spleen architecture. (**A**) Spleen sections from 8.5-month-old male WT and Lyn knockout mice were imaged via immunofluorescence microscopy. Co-occurrence of either splenomegaly or low body mass (defined in Fig. 3) is indicated (+/–). Nuclei (DAPI), B220^{+} B cells (FITC), GL7^{+} GC or activated B cells [Alexa Fluor (AF) 555], CD11b^{+} myeloid cells (AF594), and TCRβ^{+} T cells (AF647) are shown; scale bar, 500 μm. (**B**) Fourfold increased magnification showing the architecture of a representative B cell follicle, GC, and T cell zone; scale bar, 100 μm. (**C**) Spleen sections visualized by H&E staining; scale bar, 500 μm. Images are representative of $n = 3$ mice.

doctor of veterinary medicine and supporting veterinary staff. Breeding and experimental animals were genotyped via real-time PCR (Transnetyx Inc., Memphis, TN) and secondarily (where possible) by immunoblotting. All mice, including Lyn^{KO} (*53*) and Csk^{AS}, were maintained on a C57BL/6 background and bred in house. Csk^{AS} mice are hemizygous for the Csk^{AS} bacterial artificial chromosome transgene on a Csk^{KO} background (*37*, *51*). Lyn$^{+/-}$ mice are hemizygous for total Lyn expression (*52*).

Generation of LynA^{KO} and LynB^{KO} mice

CRISPR gRNAs were designed using CRISPOR.org (*73*) and purchased from IDT (Newark, NJ), and cutting efficiency was validated in NIH/3T3 cells. The LynA^{KO}(CRISPR) allele was generated using two gRNAs to induce double-strand breaks, effectively deleting 77–base pair (bp) bounding portions of the unique LynA insert in mouse *lyn* exon 2 (5′-GAUCUCUCACAUAAAUAGUU-3′) and the following intron 2 (5′-CCAUGCUCCGAUCCUACUGU-3′). The LynB^{KO}(CRISPR) allele was generated using one gRNA (5′-GUUCGGUCAGUAUUACGUAC-3′) to cut near the LynB splice site in exon 2. A donor oligonucleotide (5′-AAAAGGAAAG-ACAATCTCAATGACGATGAAGTAGATTCGAAGACTCAAC-CAcTgCGTAATACTGACCCAACTATTTATGTGAGAGATC-CAACGTCCAATAAACAGCAAAGGCCAGTAAG-3′) was supplied to template two single-nucleotide substitutions for HDR (indicated by the lowercase letters in the above sequence) that ablated the LynB splice site and an BI restriction site.

To generate the CRISPR alleles, stud C57BL/6J male mice and 3-week-old C57BL/6J female mice were purchased from The Jackson Laboratory (Bar Harbor, ME); females were housed 3 to 4 days before hormone injection. Superovulation was induced via intraperitoneal injection of 5 IU of pregnant mare serum gonadotropin, followed 48 hours later by 5 IU of human chorionic gonadotropin (National Hormone & Peptide Program, Torrance, CA). Females were then immediately mated with the stud males, and zygotes were harvested the following day and injected with Cas9 protein (30 ng/μl) and 3.5 ng/μl of each gRNA. For LynB^{KO}, the injection mixture also included single-stranded, 120-bp donor oligonucleotide (7 ng/μl) (*39*). Embryos were then implanted into female CD-1 mice (38 to 49 days old) purchased from Charles River Laboratories (Wilmington, MA).

DNA was isolated from the toes of candidate pups using the DNeasy Blood & Tissue Kit (Qiagen, Hilden, Germany) and subjected to intermediate Topo cloning (Invitrogen, Carlsbad, CA) to insert PCR products into a plasmid for PCR amplification/restriction digest and sequencing (GENEWIZ, South Plainfield, NJ). A 500-bp segment, encompassing the LynB splice site and the LynA unique insert, was amplified from each candidate using the primers 5′-ACAACCGAGATGTCCTGCT-3′ (forward) and 5′-AGCCAGAT-TATCCCTAAAATCTCTACA-3′ (reverse). SnaBI (New England Biolabs, Ipswich, MA) cleavage of WT product (recognition site TAC/GTA) generates two 250-bp fragments. In LynA^{KO}, a Cas9 double cut yielded a shorter (~423 bp) SnaBI sensitive product. In LynB^{KO}, the 500-bp PCR product was not cleavable by SnaBI.

Csk^{AS}LynB^{KO} mice were generated by breeding LynB^{KO} into our Csk$^{+/-}$ and Csk^{AS}(Csk^{KO}) strains and then crossing the progeny Csk$^{+/-}$LynB^{KO} (or Lyn^{KO}) and Csk^{AS}(Csk^{KO})Lyn^{KO} (or LynB^{KO}) together, as described previously for Csk^{AS}Lyn^{KO} (*37*), Csk^{AS}c-Cbl^{KO}, and Csk^{AS}Cbl-b^{KO} (*36*). Csk^{AS}LynA^{KO} mice were also generated in parallel.

DNA constructs, mutagenesis, and transfection of Jurkat cells

His$_6$V5-tagged mouse LynA and Myc-tagged memCsk^{AS} constructs have been described previously (*36*). Site-directed mutagenesis

(QuikChange Lightning, Agilent Technologies, Santa Clara, CA) was used to generate LynA^{V24L} from the WT LynA plasmid DNA. Mutations were confirmed via sequencing (GENEWIZ, South Plainfield, NJ).

After authentication via short tandem repeat (STR) profiling and testing negative for mycoplasma (American Type Culture Collection, Manassas, VA), Jurkat-derived JCaM1.6 T cells (*43*, *44*) were cultured in RPMI 1640 medium supplemented with 5 to 10% fetal bovine serum (FBS) (Omega Scientific, Tarzana, CA) and 2 mM glutamine, penicillin, and streptomycin (Sigma-Aldrich, St. Louis, MO). For transient transfections, cells were grown overnight in transfection medium: antibiotic-free RPMI 1640 with 10% FBS and 2 mM glutamine. Batches of 15 million cells were resuspended in transfection medium with 10 to 15 μg each plasmid DNA (LynA and memCsk^{AS}). Cells were rested and then electroporated for 10 ms at 285 V in a BTX square-wave unit (Harvard Apparatus, Holliston, MA). Cells were then resuspended in transfection medium and rested in a cell culture incubator overnight. One million live cells were then resuspended in phosphate-buffered saline (PBS) and rested for 30 min at 37°C before stimulation and analysis.

Preparation of BMDMs, BMDCs, and mast cells

Bone marrow was extracted from femora/tibiae of mice and subjected to hypotonic erythrocyte lysis. BMDMs were generated on untreated plates (BD Falcon, Bedford, MA) by culturing in Dulbecco's modified Eagle's medium (DMEM) (Corning Cellgro, Manassas, VA) containing ~10% heat-inactivated FBS (Omega Scientific, Tarzana, CA), sodium pyruvate (0.11 mg/ml), 2 mM penicillin/streptomycin/L-glutamine (Sigma-Aldrich, St. Louis, MO), and 10% CMG14-12 cell–conditioned medium as a source of macrophage colony-stimulating factor (M-CSF). After 6 or 7 days, cells were resuspended in enzyme-free EDTA buffer, replated, and rested overnight in untreated six-well plates (BD Falcon) at 1 million cells per well in unconditioned medium ± IFN-γ (25 U/ml) (PeproTech, Cranbury, NJ) (*36*, *74*) before stimulation and analysis.

BMDCs were generated on 10-cm tissue culture (TC)–treated plates (Celltreat, Pepperell, MA) in DMEM (Corning Cellgro, Manassas, VA). For DC culture, CMG-12-14 supernatant was replaced with murine granulocyte-macrophage colony-stimulating factor (GM-CSF) (10 ng/ml) and murine interleukin-4 (IL-4) (10 ng/ml) (both PeproTech), with medium refreshment on day 4. On day 7, cells were resuspended in enzyme-free EDTA buffer, replated in TC-treated 12-well plates (Celltreat, Pepperell, MA) at 1 million cells per well in DMEM + 10% FBS, and rested overnight at 37°C before analysis. In the final cell mixture, CD11c$^+$ cDCs comprised only 0.5% of live cells and PDCA1$^+$ pDCs comprised 0.1% of live cells, with the major contaminating populations being macrophages (91%) and monocytes (6%).

Bone marrow–derived mast cells were prepared as described previously (*36*, *75*), with CMG14-12 supernatant replaced by murine IL-3 (10 ng/ml; PeproTech). Cells were cultured for at least 5 weeks before lysis and analysis.

Isolation of splenic B cells, DCs, and peripheral blood monocytes

B cells were isolated from 3.5- to 4.5-month-old mice via a negative selection strategy adapted from the EasySep Mouse B Cell Isolation Kit (STEMCELL Technologies, Vancouver, Canada). Mouse spleens were disintegrated in PBS containing 2% FBS and 1 mM EDTA (PBS-FBS-EDTA) and passed through a 40-μm mesh filter. Batches of 100 million cells were resuspended in 1 ml of PBS-FBS-EDTA, mixed with normal rat serum (STEMCELL Technologies), and incubated for 10 min at room temperature (RT) with the following biotinylated antibodies from BioLegend and Tonbo Biosciences (both San Diego, CA): CD3 (BioLegend, 100244), CD64 (BioLegend, 139318), CD4 (Tonbo Biosciences, 30-0041-U100), CD8 (Tonbo Biosciences, 30-0081-U500), CD161/NK1.1 (Tonbo Biosciences, 30-5941-U500), F4/80 (Tonbo Biosciences, 30-4801-U500), Gr-1 (Tonbo Biosciences, 30-5931-U500), CD11c (Tonbo Biosciences, 30-0114-U100), and Ter119 (Tonbo Biosciences, 30-5921-U500).

Splenocytes were then incubated with magnetic MojoSort Streptavidin Nanobeads (BioLegend) and incubated for 3 min at RT. Tubes were then placed inside a column-free EasySep magnet for 3 min. Flow-through was characterized via flow cytometry: From six independent isolations, the B220$^+$ B cells comprised 76 ± 7% of live cells, with the major contaminating populations being (low-Lyn–expressing) NK cells (5 ± 3%) and eosinophils (3 ± 2%).

DCs were isolated via negative selection with the EasySep Mouse Pan-DC Enrichment Kit. From three independent isolations, CD11c$^+$ cDCs comprised 42 ± 4% of live cells and PDCA1$^+$ pDCs comprised 5 ± 1%, with the major contaminating populations being macrophages (5 ± 1%) and (low-Lyn–expressing) NK cells (1%).

Peripheral blood monocytes were isolated from 3.5- to 4.5-month-old mice by negative selection. Blood collected in heparin tubes was subjected to hypotonic lysis to remove erythrocytes. After washing, batches of 100 million cells were resuspended in 1 ml of PBS-FBS-EDTA and isolated by magnetic sorting with the EasySep Mouse Monocyte Isolation Kit (STEMCELL Technologies). Monocyte suspensions were washed and characterized via flow cytometry from six independent isolations, and the final samples contained approximately 61% CD64$^+$MerTK$^-$ monocytes, with the largest contaminants being 10% B cells and 2% (non-Lyn–expressing) T cells.

Cell stimulation and immunoblotting

Cultured cells were treated with 10 μM 3-IB-PP1 (K. Shokat, University of California San Francisco) at 37°C before placing on ice, lysing with SDS sample buffer, and preparation for immunoblotting (*74*). Approximately 0.025 million cell equivalents were run in each lane of a 7% NuPAGE tris-acetate gel (Invitrogen, Carlsbad, CA) and transferred to Immobilon-FL polyvinylidene difluoride membrane (EMD Millipore, Burlington, MA). REVERT Total Protein Stain (LI-COR Biosciences, Lincoln, NE) was used as a standard for the whole-sample protein content for quantification (*74*). After reversing the total protein staining, membranes were treated for 1 hour with Intercept (TBS) Blocking Buffer (LI-COR Biosciences) and incubated with the appropriate primary and near-infrared secondary antibodies from Cell Signaling Technology (Danvers, MA), Abcam (Cambridge, UK), ProMab Biotechnologies (Richmond, CA), R&D Systems (Minneapolis, MN), and LI-COR Biosciences (Lincoln, NE): β-actin 8H10D10 (Cell Signaling Technology, 3700), Erk1/2 3A7 (Cell Signaling Technology, 9107), Fgr 6G2 (ProMab Biotechnologies, 20318), Fyn (Cell Signaling Technology, 4023), Hck 394903 (R&D Systems, MAB3915), LynA + LynB Lyn-01 (Abcam, ab1890), Src (Cell Signaling Technology, 2108), V5 epitope tag D3H8Q (Cell Signaling Technology, 13202), phospho-Erk1/2 (pT202/pY204) D13.14.4E (Cell Signaling Technology, 4370), phospho-Zap70/Syk (pY Zap 319/Syk 352) 65E4 (Cell Signaling Technology, 2717), IRDye 800CW donkey anti-mouse IgG (LI-COR

Biosciences, NC9744100), IRDye 800CW donkey anti-rabbit IgG (LI-COR Biosciences, NC9523609), and IRDye 680RD donkey anti-mouse IgG (LI-COR Biosciences, 926-68072). Blots were visualized using an Odyssey CLx near-infrared imager (LI-COR Biosciences), and signals were background-subtracted using ImageStudio Software (LI-COR Biosciences) and corrected for whole-lane protein content (total protein stain) (*74*).

Flow cytometry

Spleens were excised from mice, mechanically disintegrated, and passed through a 70-μm mesh filter. Single-cell suspensions were then subjected to hypotonic erythrocyte lysis and resuspended in fluorescence-activated cell sorting (FACS) buffer (PBS without Ca^{2+}/Mg^{2+} supplemented with 2% FBS and 2 mM EDTA). Antibody master mixes for cell surface stains were prepared in FACS buffer, and staining was performed for 1 hour at 4 or 37°C. Cells were then fixed and permeabilized in Cytofix/Cytoperm solution (BD Biosciences, San Jose, CA) for 20 min at 4°C. After washing in BD Perm/Wash buffer, intracellular staining was performed overnight at 4°C with antibodies in Perm/Wash buffer. Following washing, samples were resuspended in PBS with 0.5% paraformaldehyde. Flow cytometry was performed on Fortessa X-30, and data were analyzed using FlowJo software. Flow cytometry antibodies were combined as appropriate from BD Biosciences (San Diego, CA), Thermo Fisher Scientific, Tonbo Biosciences, and BioLegend: B220 RA3-6B2 BUV395 (BD Biosciences), CD4 GK1.5 BUV395 (BD Biosciences), CD8a 53-6.7 BUV737 (BD Biosciences), CD11b M1/70 BUV395/A700/BUV737 (BD Biosciences), CD11c HL3 BUV737 (BD Biosciences), CD16/32 2.4G2 (Tonbo Biosciences), CD19 6D5 BV711 (BioLegend), CD21/35 7E9 fluorescein isothiocyanate (FITC) (BioLegend), CD23 B3B4 phycoerythrin (PE) (BioLegend), CD25 PC61 BV605 (BioLegend), CD38 90 A700 (BioLegend), CD44 IM7 peridinin chlorophyll protein (PerCP)–Cy5.5 (Tonbo Biosciences), CD45 30-F11 A700/BUV496 (BioLegend), CD62L MEL-14 BV510 (BioLegend), CD64 X54-5/7.1 BV711 (BioLegend), CD69 H1.2F3 FITC (Tonbo Biosciences), CD80 B7-1/16-10A1 PE (Tonbo Biosciences), CD86 B7-2/PO3.1 PE (Tonbo Biosciences), CD93 AA4.1 allophycocyanin (APC) (BioLegend), CD138 281-2 BV421 (BioLegend), CD170/Siglec-F S17007L FITC (BioLegend), CD185 L138D7 PE (BioLegend), CD206 C068C2 BV650 (BioLegend), FoxP3 3G3 PE-Cy7 (Tonbo Biosciences), Ghost Dye Red 780 (Tonbo Biosciences), GL7 PerCP-Cy5.5 (BioLegend), I-A/I-E M5/114.15.2 BV510 (BioLegend), IgD 11-26C.1 BV786 (BD Biosciences), IgM RMM-1 PE-Cy7 (BioLegend), Intracellular Ig 550589 PE (BD Biosciences), Ly6C HK1.3 BV785 (BioLegend), Ly6G 1A8 PerCP-Cy5.5 (Tonbo Biosciences), MerTK DS5MMER PE-Cy7 (Thermo Fisher Scientific), NK1 PK136 BV421 (BioLegend), PD-1 29F.1A12 BV785 (BioLegend), PDCA-1 927 BV421 (BioLegend), TCRβ H57-597 FITC/APC (Tonbo Biosciences), and XCR1 ZET FITC and APC (BioLegend).

Immunofluorescence microscopy

Spleens and kidneys were excised from aged mice and frozen in optimal cutting temperature (OCT) compound before sectioning. Sections of 5-μm thickness were cut from each block and kept frozen (*76*). Before staining, sections were dried for 30 min, fixed for 15 min in ice-cold acetone, dried for 10 min, and washed for 5 min in PBS-based buffer with 0.5% bovine serum albumin (BSA). Sections were then blocked for 1 hour with 2% BSA and 1:100 Fc Shield (Tonbo Biosciences) in PBS and then washed for 5 min. Spleen sections were further blocked using an endogenous biotin blocking kit (Invitrogen) and washed 3 × 5 min. Spleen sections were then stained overnight at 4°C with CD11b-AF594 (M1/70), TCRβ-AF647 (H57-597), GL7-biotin (GL7), and B220-FITC (RA3-6B2). Kidney sections were stained with C3-FITC (RmC11H9) and goat anti-mouse FC–Texas Red (Jackson ImmunoResearch). Stained sections were washed 3 × 5 min. Spleen sections were subsequently stained for 1 hour with Streptavidin–DyLight 550 (Thermo Fisher Scientific) secondary antibody and washed. Sections were mounted with ProLong Gold DAPI (4′,6-diamidino-2-phenylindole)–infused mounting media (Cell Signaling Technology) and glass coverslips. Slides were imaged on a Leica DM6000B fluorescence microscope at ×5, ×20, or ×40 magnification. Sixteen tiled images from each kidney were merged for analysis. C3/Ig deposition was quantified in batch using Imaris software (Oxford Instruments, Abingdon, UK).

H&E staining and scoring

Spleen and kidney sections were H&E-stained for pathological assessment of tissue architecture and glomerulonephritis. Sections were dried for 30 min at RT and fixed for 15 min in ice-cold acetone. Sections were then rinsed for 2 min in PBS, stained for 2 min with hematoxylin quick stain (Vector Laboratories, Burlingame, CA), and rinsed again in water until clear. Sections were then stained for 1 min with eosin (Vector), rinsed 2 × 5 min in 95% ethanol, rinsed 2 × 5 min in 100%, and cleared for 10 min in a xylene mixture. Slides were mounted with VectaMount medium (Vector Laboratories). Kidney images were deidentified and sent to a pathologist for disease scoring of glomerulonephritis and interstitial nephritis (*77*). Scoring was performed on a 0 to 3 scale (0 = absent, 1 = mild, 2 = severe) based on glomerular size, hypercellularity, and sclerosis; interstitial disease was assessed on the basis of the degree of inflammatory infiltrate and alteration in tissue architecture.

Trichrome staining

Kidney or spleen sections were dried for 30 min and fixed for 10 min in 4% paraformaldehyde in PBS at RT. The Trichrome Stain Kit (Abcam ab150686) was then used to stain sections according to the manufacturer's protocol. Briefly, sections were incubated for 1 hour at 60°C in Bouin's fluid, rinsed, and incubated for 5 min in Weigert's hematoxylin, rinsed, stained for 15 min with Biebrich scarlet/acid fuschin, rinsed, incubated for 10 min in phosphomolybdic/phosphotungstic acid, stained for 15 min with aniline blue, rinsed in deionized water, and then incubated for 5 min in 1% acetic acid. Sections were then dehydrated with two rinses with 95% ethanol and two rinses with 100% ethanol, cleared with xylene, and mounted with VectaMount medium (Vector Laboratories, Burlingame, CA). Slides were imaged on a bright-field microscope and analyzed using NIH ImageJ Fiji.

Serum collection from mice

Blood was harvested via venipuncture from the submandibular vein of mice or via retroorbital bleed and allowed to clot at RT for 90 min, after which it was spun at 4000 rpm at 4°C for 10 min. The resulting serum supernatant was then aliquoted and placed on ice for immediate use or stored at −80°C.

BAFF analysis

The Quantikine ELISA (enzyme-linked immunosorbent assay) Kit for Mouse BAFF/BLyS/TNFSF13B (R&D Systems, catalog no. MBLYS0)

was used to quantify serum levels of BAFF. Assay Diluent RD1N (80 µl) was added to each well of a microplate. Standard or sample (40 µl, after 1:50 dilution in Calibrator Diluent RD6-12) was added to each well in technical duplicate. Other reagents were prepared according to the manufacturer's instructions. Samples were incubated for 2 hours at RT on a horizontal orbital shaker at 225 rpm. Each well was then washed 5×. Mouse BAFF/BLyS Conjugate (120 µl) was added to each well and incubated for 2 hours at RT on the orbital shaker. After washing, 120 µl of Substrate Solution was added to each well and incubated for 30 min in the dark. Stop solution (120 µl) was then added to each well. Optical density (OD) at 450 nm was measured immediately using the Bio-Rad iMark Microplate Reader. The average OD from each sample was converted to picogram per milliliter value with reference to the standard curve and correction for dilution.

IgM analysis

Wells in polystyrene 96-well plates were coated with 50 µl of anti-mouse IgM Fab2 (prepared at 1 µg/ml in PBS), incubated overnight, washed 6× with distilled water, blocked for 1 hour at RT with 50 µl of PBS-BB (PBS without Ca^{2+}/Mg^{2+}, 0.05% Tween 20, and 1% BSA), and initiated with 50 µl of 1:60,000 diluted serum. After incubation for 2 hours at RT, wells were washed 6×. Biotinylated anti-mouse IgM (50 µl at 500 ng/ml) was then added to each well and incubated for 1 hour at RT. After washing, 50 µl of streptavidin–horseradish peroxidase (diluted 1:40 in PBS-BB) was added to each well and incubated for 1 hour at RT. After washing, ELISA results were visualized by adding 50 µl of trimethylboron:peroxide and stopped with 50 µl of sulfuric acid (1 N). Relative amounts of IgM were determined by measuring the OD at 450 nm using the Bio-Rad iMark Microplate Reader.

ANA detection

Kallestad HEp-2 (Bio-Rad, catalog no. 30472) was used to detect ANA staining according to the manufacturer's instruction, modified to detect mouse IgG. Briefly, wells were incubated with 40 µl of mouse serum, diluted 40× in PBS with 1% BSA, at RT for 20 min. After incubation, slides were washed in PBS for 10 min and incubated with 30 µl of FITC-labeled goat anti-mouse IgG (Jackson ImmunoResearch, catalog no. 115-095-164) diluted 200× in DAPI for 20 min at RT, followed by a 10-min PBS wash. Slides were then mounted and coverslipped and viewed on an Olympus BX51 fluorescent microscope equipped with a digital camera and DP-BSW software (Olympus). Images were quantified, pseudo-colored, and merged using ImageJ software (NIH) with the Fiji plugin.

Statistical analyses

Statistical analysis was performed using Prism software (GraphPad, La Jolla, CA). Significance was typically assessed using one-way analysis of variance (ANOVA) with Tukey's multiple comparisons test, unless otherwise indicated. For cellularity analyses, outliers were identified using robust regression and outlier removal (ROUT) analysis ($Q = 1\%$). Student's t test was used for simple, two-way comparisons. Contingency data were assessed using two-sided Fisher's exact test with Welch's correction, with and without Bonferroni correction. To meet the test conditions, data were binarized as indicated by combining no/mild disease groups or mild/severe groups. Error bars typically reflect 95% confidence interval (CI) or SEM, and n values reflect individual animals, pooled from multiple independent experiments.

SUPPLEMENTARY MATERIALS

Supplementary material for this article is available at https://science.org/doi/10.1126/sciadv.abj5227

View/request a protocol for this paper from *Bio-protocol*.

REFERENCES AND NOTES

1. Y. Yamanashi, Y. Fukui, B. Wongsasant, Y. Kinoshita, Y. Ichimori, K. Toyoshima, T. Yamamoto, Activation of Src-like protein-tyrosine kinase Lyn and its association with phosphatidylinositol 3-kinase upon B-cell antigen receptor-mediated signaling. *Proc. Natl. Acad. Sci. U.S.A.* **89**, 1118–1122 (1992).
2. K. G. Smith, D. M. Tarlinton, G. M. Doody, M. L. Hibbs, D. T. Fearon, Inhibition of the B cell by CD22: A requirement for Lyn. *J. Exp. Med.* **187**, 807–811 (1998).
3. E. J. Brodie, S. Infantino, M. S. Y. Low, D. M. Tarlinton, Lyn, lupus, and (B) lymphocytes, a lesson on the critical balance of kinase signaling in immunity. *Front. Immunol.* **9**, 401 (2018).
4. P. Scapini, S. Pereira, H. Zhang, C. A. Lowell, Multiple roles of Lyn kinase in myeloid cell signaling and function. *Immunol. Rev.* **228**, 23–40 (2009).
5. B. F. Brian, T. S. Freedman, The Src-family kinase lyn in immunoreceptor signaling. *Endocrinology* **162**, bqab152 (2021).
6. J. T. Greene, B. F. Brian, S. E. Senevirathne, T. S. Freedman, Regulation of myeloid-cell activation. *Curr. Opin. Immunol.* **73**, 34–42 (2021).
7. V. W. Chan, C. A. Lowell, A. L. DeFranco, Defective negative regulation of antigen receptor signaling in Lyn-deficient B lymphocytes. *Curr. Biol.* **8**, 545–553 (1998).
8. A. J. Gross, J. R. Lyandres, A. K. Panigrahi, E. T. Prak, A. L. DeFranco, Developmental acquisition of the Lyn-CD22-SHP-1 inhibitory pathway promotes B cell tolerance. *J. Immunol.* **182**, 5382–5392 (2009).
9. J. Ma, C. L. Abram, Y. Hu, C. A. Lowell, CARD9 mediates dendritic cell-induced development of Lyn deficiency-associated autoimmune and inflammatory diseases. *Sci. Signal.* **12**, eaao3829 (2019).
10. T. Ban, G. R. Sato, A. Nishiyama, A. Akiyama, M. Takasuna, M. Umehara, S. Suzuki, M. Ichino, S. Matsunaga, A. Kimura, Y. Kimura, H. Yanai, S. Miyashita, J. Kuromitsu, K. Tsukahara, K. Yoshimatsu, I. Endo, T. Yamamoto, H. Hirano, A. Ryo, T. Taniguchi, T. Tamura, Lyn kinase suppresses the transcriptional activity of IRF5 in the TLR-MyD88 pathway to restrain the development of autoimmunity. *Immunity* **45**, 319–332 (2016).
11. C. Lamagna, P. Scapini, J. A. van Ziffle, A. L. DeFranco, C. A. Lowell, Hyperactivated MyD88 signaling in dendritic cells, through specific deletion of Lyn kinase, causes severe autoimmunity and inflammation. *Proc. Natl. Acad. Sci. U.S.A.* **110**, E3311–E3320 (2013).
12. S. Keck, M. Freudenberg, M. Huber, Activation of murine macrophages via TLR2 and TLR4 is negatively regulated by a Lyn/PI3K module and promoted by SHIP1. *J. Immunol.* **184**, 5809–5818 (2010).
13. R. Lu, G. S. Vidal, J. A. Kelly, A. M. D. Vega, X. K. Howard, S. R. Macwana, N. Dominguez, W. Klein, C. Burrell, I. T. Harley, K. M. Kaufman, G. R. Bruner, K. L. Moser, P. M. Gaffney, G. S. Gilkeson, E. K. Wakeland, Q.-Z. Li, C. D. Langefeld, M. C. Marion, J. Divers, G. S. Alarcón, E. E. Brown, R. P. Kimberly, J. C. Edberg, R. R. Goldman, J. D. Reveille, G. Mc Gwin Jr., L. M. Vilá, M. A. Petri, S.-C. Bae, S.-K. Cho, S.-Y. Bang, I. Kim, C.-B. Choi, J. Martin, T. J. Vyse, J. T. Merrill, J. B. Harley, M. E. A. Riquelme; BIOLUPUS, GENLES Multicenter Collaborations, S. K. Nath, J. A. James, J. M. Guthridge, Genetic associations of LYN with systemic lupus erythematosus. *Genes Immun.* **10**, 397–403 (2009).
14. International Consortium for Systemic Lupus Erythematosus Genetics (SLEGEN), J. B. Harley, M. E. A.-Riquelme, L. A. Criswell, C. O. Jacob, R. P. Kimberly, K. L. Moser, B. P. Tsao, T. J. Vyse, C. D. Langefeld, S. K. Nath, J. M. Guthridge, B. L. Cobb, D. B. Mirel, M. C. Marion, A. H. Williams, J. Divers, W. Wang, S. G. Frank, B. Namjou, S. B. Gabriel, A. T. Lee, P. K. Gregersen, T. W. Behrens, K. E. Taylor, M. Fernando, R. Zidovetzki, P. M. Gaffney, J. C. Edberg, J. D. Rioux, J. O. Ojwang, J. A. James, J. T. Merrill, G. S. Gilkeson, M. F. Seldin, H. Yin, E. C. Baechler, Q.-Z. Li, E. K. Wakeland, G. R. Bruner, K. M. Kaufman, J. A. Kelly, Genome-wide association scan in women with systemic lupus erythematosus identifies susceptibility variants in ITGAM, PXK, KIAA1542 and other loci. *Nat. Genet.* **40**, 204–210 (2008).
15. S. N. Liossis, E. E. Solomou, M. A. Dimopoulos, P. Panayiotidis, M. M. Mavrikakis, P. P. Sfikakis, B cell kinase lyn deficiency in patients with systemic lupus erythematosus. *J. Invest. Med.* **49**, 157–165 (2001).
16. F. Flores-Borja, P. S. Kabouridis, E. C. Jury, D. A. Isenberg, R. A. Mageed, Decreased Lyn expression and translocation to lipid raft signaling domains in B lymphocytes from patients with systemic lupus erythematosus. *Arthritis Rheum.* **52**, 3955–3965 (2005).
17. M. L. Hibbs, D. M. Tarlinton, J. Armes, D. Grail, G. Hodgson, R. Maglitto, S. A. Stacker, A. R. Dunn, Multiple defects in the immune system of Lyn-deficient mice, culminating in autoimmune disease. *Cell* **83**, 301–311 (1995).
18. K. W. Harder, L. M. Parsons, J. Armes, N. Evans, N. Kountouri, R. Clark, C. Quilici, D. Grail, G. S. Hodgson, A. R. Dunn, M. L. Hibbs, Gain- and loss-of-function Lyn mutant mice define a critical inhibitory role for Lyn in the myeloid lineage. *Immunity* **15**, 603–615 (2001).

19. C. C. K. Yu, T. S. B. Yen, C. A. Lowell, A. L. DeFranco, Lupus-like kidney disease in mice deficient in the Src family tyrosine kinases Lyn and Fyn. *Curr. Biol.* **11**, 34–38 (2001).
20. K. M. Pollard, Gender differences in autoimmunity associated with exposure to environmental factors. *J. Autoimmun.* **38**, J177–J186 (2012).
21. A. V. Rubtsov, K. Rubtsova, J. W. Kappler, P. Marrack, Genetic and hormonal factors in female-biased autoimmunity. *Autoimmun. Rev.* **9**, 494–498 (2010).
22. O. L. Quintero, M. J. Amador-Patarroyo, G. Montoya-Ortiz, A. Rojas-Villarraga, J. M. Anaya, Autoimmune disease and gender: Plausible mechanisms for the female predominance of autoimmunity. *J. Autoimmun.* **38**, J109–J119 (2012).
23. C. M. Syrett, M. C. Anguera, When the balance is broken: X-linked gene dosage from two X chromosomes and female-biased autoimmunity. *J. Leukoc. Biol.* **106**, 919–932 (2019).
24. A. L. Fink, K. Engle, R. L. Ursin, W. Y. Tang, S. L. Klein, Biological sex affects vaccine efficacy and protection against influenza in mice. *Proc. Natl. Acad. Sci. U.S.A.* **115**, 12477–12482 (2018).
25. S. L. Klein, A. Hodgson, D. P. Robinson, Mechanisms of sex disparities in influenza pathogenesis. *J. Leukoc. Biol.* **92**, 67–73 (2012).
26. T. Ozcelik, X chromosome inactivation and female predisposition to autoimmunity. *Clin. Rev. Allergy Immunol.* **34**, 348–351 (2008).
27. M. Souyris, C. Cenac, P. Azar, D. Daviaud, A. Canivet, S. Grunenwald, C. Pienkowski, J. Chaumeil, J. E. Mejía, J.-C. Guéry, TLR7 escapes X chromosome inactivation in immune cells. *Sci. Immunol.* **3**, eaap8855 (2018).
28. E. Ricker, M. Manni, D. Flores-Castro, D. Jenkins, S. Gupta, J. Rivera-Correa, W. Meng, A. M. Rosenfeld, T. Pannellini, M. Bachu, Y. Chinenov, P. K. Sculco, R. Jessberger, E. T. Luning Prak, A. B. Pernis, Altered function and differentiation of age-associated B cells contribute to the female bias in lupus mice. *Nat. Commun.* **12**, 4813 (2021).
29. Y. Hao, P. O'Neill, M. S. Naradikian, J. L. Scholz, M. P. Cancro, A B-cell subset uniquely responsive to innate stimuli accumulates in aged mice. *Blood* **118**, 1294–1304 (2011).
30. A. V. Rubtsov, K. Rubtsova, A. Fischer, R. T. Meehan, J. Z. Gillis, J. W. Kappler, P. Marrack, Toll-like receptor 7 (TLR7)-driven accumulation of a novel CD11c^{+} B-cell population is important for the development of autoimmunity. *Blood* **118**, 1305–1315 (2011).
31. S. A. Jenks, K. S. Cashman, E. Zumaquero, U. M. Marigorta, A. V. Patel, X. Wang, D. Tomar, M. C. Woodruff, Z. Simon, R. Bugrovsky, E. L. Blalock, C. D. Scharer, C. M. Tipton, C. Wei, S. S. Lim, M. Petri, T. B. Niewold, J. H. Anolik, G. Gibson, F. E.-H. Lee, J. M. Boss, F. E. Lund, I. Sanz, Distinct effector b cells induced by unregulated toll-like receptor 7 contribute to pathogenic responses in systemic lupus erythematosus. *Immunity* **49**, 725, 739.e6 (2018).
32. C. Lamagna, Y. Hu, A. L. DeFranco, C. A. Lowell, B cell-specific loss of Lyn kinase leads to autoimmunity. *J. Immunol.* **192**, 919–928 (2014).
33. T. L. Yi, J. B. Bolen, J. N. Ihle, Hematopoietic cells express two forms of lyn kinase differing by 21 amino acids in the amino terminus. *Mol. Cell. Biol.* **11**, 2391–2398 (1991).
34. D. Alvarez-Errico, Y. Yamashita, R. Suzuki, S. Odom, Y. Furumoto, T. Yamashita, J. Rivera, Functional analysis of Lyn kinase A and B isoforms reveals redundant and distinct roles in Fc ε RI-dependent mast cell activation. *J. Immunol.* **184**, 5000–5008 (2010).
35. G. Tornillo, C. Knowlson, H. Kendrick, J. Cooke, H. Mirza, I. Aurrekoetxea-Rodríguez, M. D. M. Vivanco, N. E. Buckley, A. Grigoriadis, M. J. Smalley, Dual mechanisms of LYN kinase dysregulation drive aggressive behavior in breast cancer cells. *Cell Rep.* **25**, 3674–3692.e10 (2018).
36. B. F. Brian IV, A. S. Jolicoeur, C. R. Guerrero, M. G. Nunez, Z. E. Sychev, S. A. Hegre, P. Sætrom, N. Habib, J. M. Drake, K. L. Schwertfeger, T. S. Freedman, Unique-region phosphorylation targets LynA for rapid degradation, tuning its expression and signaling in myeloid cells. *eLife* **8**, e46043 (2019).
37. T. S. Freedman, Y. X. Tan, K. M. Skrzypczynska, B. N. Manz, F. V. Sjaastad, H. S. Goodridge, C. A. Lowell, A. Weiss, LynA regulates an inflammation-sensitive signaling checkpoint in macrophages. *eLife* **4**, e09183 (2015).
38. X. Ma, C. Chen, J. Veevers, X. M. Zhou, R. S. Ross, W. Feng, J. Chen, CRISPR/Cas9-mediated gene manipulation to create single-amino-acid-substituted and floxed mice with a cloning-free method. *Sci. Rep.* **7**, 42244 (2017).
39. H. Miura, R. M. Quadros, C. B. Gurumurthy, M. Ohtsuka, Easi-CRISPR for creating knock-in and conditional knockout mouse models using long ssDNA donors. *Nat. Protoc.* **13**, 195–215 (2018).
40. F. Madeira, Y. M. Park, J. Lee, N. Buso, T. Gur, N. Madhusoodanan, P. Basutkar, A. R. N. Tivey, S. C. Potter, R. D. Finn, R. Lopez, The EMBL-EBI search and sequence analysis tools APIs in 2019. *Nucleic Acids Res.* **47**, W636–W641 (2019).
41. E. Gasteiger, A. Gattiker, C. Hoogland, I. Ivanyi, R. D. Appel, A. Bairoch, ExPASy: The proteomics server for in-depth protein knowledge and analysis. *Nucleic Acids Res.* **31**, 3784–3788 (2003).
42. F. Supek, B. Lehner, R. G. H. Lindeboom, To NMD or not to NMD: Nonsense-mediated mRNA decay in cancer and other genetic diseases. *Trends Genet.* **37**, 657–668 (2021).
43. M. A. Goldsmith, A. Weiss, Isolation and characterization of a T-lymphocyte somatic mutant with altered signal transduction by the antigen receptor. *Proc. Natl. Acad. Sci. U.S.A.* **84**, 6879–6883 (1987).
44. D. B. Straus, A. Weiss, Genetic evidence for the involvement of the lck tyrosine kinase in signal transduction through the T cell antigen receptor. *Cell* **70**, 585–593 (1992).
45. T. Okuzumi, G. S. Ducker, C. Zhang, B. Aizenstein, R. Hoffman, K. M. Shokat, Synthesis and evaluation of indazole based analog sensitive Akt inhibitors. *Mol. Biosyst.* **6**, 1389–1402 (2010).
46. T. Okuzumi, D. Fiedler, C. Zhang, D. C. Gray, B. Aizenstein, R. Hoffman, K. M. Shokat, Inhibitor hijacking of Akt activation. *Nat. Chem. Biol.* **5**, 484–493 (2009).
47. J. R. Schoenborn, Y. X. Tan, C. Zhang, K. M. Shokat, A. Weiss, Feedback circuits monitor and adjust basal Lck-dependent events in T cell receptor signaling. *Sci. Signal.* **4**, ra59 (2011).
48. M. T. Brown, J. A. Cooper, Regulation, substrates and functions of src. *Biochim. Biophys. Acta* **1287**, 121–149 (1996).
49. L. M. Chow, A. Veillette, The Src and Csk families of tyrosine protein kinases in hemopoietic cells. *Semin. Immunol.* **7**, 207–226 (1995).
50. N. Yokoyama, W. T. Miller, Identification of residues involved in v-Src substrate recognition by site-directed mutagenesis. *FEBS Lett.* **456**, 403–408 (1999).
51. Y. X. Tan, B. N. Manz, T. S. Freedman, C. Zhang, K. M. Shokat, A. Weiss, Inhibition of the kinase Csk in thymocytes reveals a requirement for actin remodeling in the initiation of full TCR signaling. *Nat. Immunol.* **15**, 186–194 (2014).
52. E. Tsantikos, M. J. Maxwell, N. Kountouri, K. W. Harder, D. M. Tarlinton, M. L. Hibbs, Genetic interdependence of Lyn and negative regulators of B cell receptor signaling in autoimmune disease development. *J. Immunol.* **189**, 1726–1736 (2012).
53. V. W. Chan, F. Meng, P. Soriano, A. L. DeFranco, C. A. Lowell, Characterization of the B lymphocyte populations in Lyn-deficient mice and the role of Lyn in signal initiation and down-regulation. *Immunity* **7**, 69–81 (1997).
54. E. Yamada, J. E. Pessin, I. J. Kurland, G. J. Schwartz, C. C. Bastie, Fyn-dependent regulation of energy expenditure and body weight is mediated by tyrosine phosphorylation of LKB1. *Cell Metab.* **11**, 113–124 (2010).
55. M. Knoll, S. Winther, A. Natarajan, H. Yang, M. Jiang, P. Thiru, A. Shahsafaei, T. E. Chavarria, D. W. Lamming, L. Sun, J. B. Hansen, H. F. Lodish, SYK kinase mediates brown fat differentiation and activation. *Nat. Commun.* **8**, 2115 (2017).
56. A. J. Gross, I. Proekt, A. L. DeFranco, Elevated BCR signaling and decreased survival of Lyn-deficient transitional and follicular B cells. *Eur. J. Immunol.* **41**, 3645–3655 (2011).
57. M. E. Roberts, M. Barvalia, J. A. F. D. Silva, R. A. Cederberg, W. Chu, A. Wong, D. C. Tai, S. Chen, I. Matos, J. J. Priatel, P. R. Cullis, K. W. Harder, Deep phenotyping by mass cytometry and single cell rna-sequencing reveals Lyn regulated signaling profiles underlying monocyte subset heterogeneity and life span. *Circ. Res.* **126**, e61–e79 (2020).
58. S. H. Naik, P. Sathe, H.-Y. Park, D. Metcalf, A. I. Proietto, A. Dakic, S. Carotta, M. O'Keeffe, M. Bahlo, A. Papenfuss, J.-Y. Kwak, L. Wu, K. Shortman, Development of plasmacytoid and conventional dendritic cell subtypes from single precursor cells derived in vitro and in vivo. *Nat. Immunol.* **8**, 1217–1226 (2007).
59. S. P. Nobs, C. Schneider, M. G. Dietrich, T. Brocker, A. Rolink, E. Hirsch, M. Kopf, PI3-kinase-γ has a distinct and essential role in lung-specific dendritic cell development. *Immunity* **43**, 674–689 (2015).
60. S. H. Naik, D. Metcalf, A. van Nieuwenhuijze, I. Wicks, L. Wu, M. O'Keeffe, K. Shortman, Intrasplenic steady-state dendritic cell precursors that are distinct from monocytes. *Nat. Immunol.* **7**, 663–671 (2006).
61. P. Scapini, Y. Hu, C.-L. Chu, T.-S. Migone, A. L. Defranco, M. A. Cassatella, C. A. Lowell, Myeloid cells, BAFF, and IFN-γ establish an inflammatory loop that exacerbates autoimmunity in Lyn-deficient mice. *J. Exp. Med.* **207**, 1757–1773 (2010).
62. C. M. Coquery, N. S. Wade, W. M. Loo, J. M. Kinchen, K. M. Cox, C. Jiang, K. S. Tung, L. D. Erickson, Neutrophils contribute to excess serum BAFF levels and promote CD4^{+} T cell and B cell responses in lupus-prone mice. *PLOS ONE* **9**, e102284 (2014).
63. R. Parsa, H. Lund, A.-M. Georgoudaki, X.-M. Zhang, A. O. G.-Cacais, D. Grommisch, A. Warnecke, A. L. Croxford, M. Jagodic, B. Becher, M. C. I. Karlsson, R. A. Harris, BAFF-secreting neutrophils drive plasma cell responses during emergency granulopoiesis. *J. Exp. Med.* **213**, 1537–1553 (2016).
64. D. Giordano, R. Kuley, K. E. Draves, K. Roe, U. Holder, N. V. Giltiay, E. A. Clark, BAFF produced by neutrophils and dendritic cells is regulated differently and has distinct roles in antibody responses and protective immunity against West Nile virus. *J. Immunol.* **204**, 1508–1520 (2020).
65. F. M. Harris, K. A. Meagher, M. Zhong, B. J. Daniel, M. Eckersdorff, J. A. Green, V. Voronina, C. Guo, A. Limnander, L. E. Macdonald, Flow cytometric characterization of murine B cell development. *J. Vis. Exp.* **22**, 61565 (2021).
66. J. Zikherman, R. Parameswaran, A. Weiss, Endogenous antigen tunes the responsiveness of naive B cells but not T cells. *Nature* **489**, 160–164 (2012).
67. R. J. Cornall, J. G. Cyster, M. L. Hibbs, A. R. Dunn, K. L. Otipoby, E. A. Clark, C. C. Goodnow, Polygenic autoimmune traits: Lyn, CD22, and SHP-1 are limiting elements of a biochemical pathway regulating BCR signaling and selection. *Immunity* **8**, 497–508 (1998).

68. E. Tsantikos, S. A. Oracki, C. Quilici, G. P. Anderson, D. M. Tarlinton, M. L. Hibbs, Autoimmune disease in Lyn-deficient mice is dependent on an inflammatory environment established by IL-6. *J. Immunol.* **184**, 1348–1360 (2010).
69. D. Lankar, H. V.-Schneider, V. Briken, T. Yokozeki, G. Raposo, C. Bonnerot, Dynamics of major histocompatibility complex class II compartments during B cell receptor-mediated cell activation. *J. Exp. Med.* **195**, 461–472 (2002).
70. H. Nishizumi, I. Taniuchi, Y. Yamanashi, D. Kitamura, D. Ilic, S. Mori, T. Watanabe, T. Yamamoto, Impaired proliferation of peripheral B cells and indication of autoimmune disease in lyn-deficient mice. *Immunity* **3**, 549–560 (1995).
71. M. Noviski, J. L. Mueller, A. Satterthwaite, L. A. Garrett-Sinha, F. Brombacher, J. Zikherman, IgM and IgD B cell receptors differentially respond to endogenous antigens and control B cell fate. *eLife* **7**, e35074 (2018).
72. S. A. Elmore, Histopathology of the lymph nodes. *Toxicol. Pathol.* **34**, 425–454 (2006).
73. J. P. Concordet, M. Haeussler, CRISPOR: Intuitive guide selection for CRISPR/Cas9 genome editing experiments and screens. *Nucleic Acids Res.* **46**, W242–W245 (2018).
74. B. F. Brian, C. R. Guerrero, T. S. Freedman, Immunopharmacology and quantitative analysis of tyrosine kinase signaling. *Curr. Protoc. Immunol.* **130**, e104 (2020).
75. J. Kalesnikoff, S. J. Galli, Antiinflammatory and immunosuppressive functions of mast cells. *Methods Mol. Biol.* **677**, 207–220 (2011).
76. S. Cheng, S. Fu, Y. M. Kim, W. Song, Y. Li, Y. Xue, J. Yi, L. Tian, Single-cell cytometry via multiplexed fluorescence prediction by label-free reflectance microscopy. *Sci. Adv.* **7**, eabe0431 (2021).
77. Z. Hua, A. J. Gross, C. Lamagna, N. Ramos-Hernández, P. Scapini, M. Ji, H. Shao, C. A. Lowell, B. Hou, A. L. DeFranco, Requirement for MyD88 signaling in B cells and dendritic cells for germinal center anti-nuclear antibody production in Lyn-deficient mice. *J. Immunol.* **192**, 875–885 (2014).

Acknowledgments: We thank A. Bagchi, Y. You, the University of Minnesota Mouse Genetics Laboratory, and the University of Minnesota Genome Engineering Shared Resource for technical assistance; K. Shokat and F. Rutaganira for supplying the Csk^{AS} inhibitor 3-IB-PP1; J. Williams and J. Mitchell for microscopy advice and assistance; and J. Zikherman, M. Headley, J. Hamerman, A. O'Rourke, C. Abram, M. Jenkins, K. Pape, G. Randolph, J. Brooks, C. Sellner, B. Burbach, K. Schwertfeger, M. Farrar, C. Lange, and J. Connett for valuable protocols, feedback, and discussion. **Funding:** This work was supported by NIH grant R01AR073966 (to T.S.F.), NIH supplement 3R01AR073966-03S1 (to T.S.F.), NIH grant R03AI130978 (to T.S.F.), NIH grant T32DA007097 (to B.F.B.), NIH grant T32CA009138 (to M.L.S. and J.T.G.), American Cancer Society–Kirby Foundation Postdoc Fellowship PF-21-068-01-LIB (to J.T.G.), University of Minnesota Center for Immunology New Mouse Award (to T.S.F.), University of Minnesota Foundation Equipment Award E-0918-01 (to T.S.F.), and University of Minnesota Center for Autoimmune Diseases Research Pilot Grant (to T.S.F.) **Author contributions:** Conceptualization: B.F.B. and T.S.F. Methodology: B.F.B., J.T.G., M.L.S., A.J.L., J.L.A., B.L.R., B.S.M., C.A.L., B.A.B., and T.S.F. Investigation: B.F.B., M.L.S., J.T.G., O.L.F., S.E.S., A.J.L., L.A.R., J.L.A., M.G.N., W.L.S., C.A.L., and T.S.F. Visualization: B.F.B., J.T.G., J.L.A., and T.S.F. Funding acquisition: B.F.B., J.T.G., M.L.S., and T.S.F. Project administration: T.S.F. Supervision: T.S.F. Writing—original draft: B.F.B. and T.S.F. Writing—review and editing: B.F.B., M.L.S., J.T.G., O.L.F., S.E.S., A.J.L., L.A.R., J.L.A., M.G.N., W.L.S., B.L.R., B.S.M., C.A.L., B.A.B., and T.S.F. **Competing interests:** The authors declare that they have no competing interests. **Data and materials availability:** All data needed to evaluate the conclusions in the paper are present in the paper and/or the Supplementary Materials.

Submitted 18 May 2021
Accepted 8 March 2022
Published 22 April 2022
10.1126/sciadv.abj5227

A dominant function of LynB kinase in preventing autoimmunity

Ben F. Brian IVMonica L. SauerJoseph T. GreeneS. Erandika SenevirathneAnders J. LindstedtOlivia L. FunkBrian L. RuisLuis A. RamirezJennifer L. AugerWhitney L. SwansonMyra G. NunezBranden S. MoriarityClifford A. LowellBryce A. BinstadtTanya S. Freedman

Sci. Adv., 8 (16), eabj5227.

Science Advances
AAAS

Supplementary Materials for

A dominant function of LynB kinase in preventing autoimmunity

Ben F. Brian IV, Monica L. Sauer, Joseph T. Greene, S. Erandika Senevirathne, Anders J. Lindstedt, Olivia L. Funk, Brian L. Ruis, Luis A. Ramirez, Jennifer L. Auger, Whitney L. Swanson, Myra G. Nunez, Branden S. Moriarity, Clifford A. Lowell, Bryce A. Binstadt, Tanya S. Freedman*

*Corresponding author. Email: tfreedma@umn.edu

Published 22 April 2022, *Sci. Adv.* **8**, eabj5227 (2022)
DOI: 10.1126/sciadv.abj5227

This PDF file includes:

Figs. S1 to S21

A. WT mouse *Lyn* (genomic DNA sequence)

5′ region of exon 2 (shared by LynA & LynB)
exon 2 LynB splice donor site (GT) & SnaBI restriction site (TACGTA)
3′ region of exon 2 (LynA only)
intron
exon 3 (shared)
exon 4

```
ATGGGATGTATTAAATCAAAAAGGAAAGACAATCTCAATGACGATGAAGTAGATTCGAAGACTCAACCAGTACGTAATACTGACCG
AACTATTTATGTGAGAGATCCAACGTCCAATAAACAGCAAAGGCCAgtaagtagactagtctcaggggagaaatcccacagtagga
tcggagcatggctgtgcagcctaaaccccaatctttgcatgccatatatatatacacatatataaattga…ttgctgctgttagga
aaatgatatgcatgcgagaagaaaactatgatcatgacttttgttcctctaacaaatactcttccatagGTTCCTGAATTTCATCT
TTTACCAGGACAGAGATTTCAAACAAAAGgtatgtttcctaaccaacataattcatgttttgtttgtcattgcggaaaaatacaca
caacacaagtttatcacagtttcagtcactgttttcaatgtcaagttctgaacaggaagtaca…ATCCAGAGGAACAAGGTGACAT
TGTGGTGGCCTTATACCCTTATGATGGCATCCACCCAGATGACTTGTCCTTCAAGAAAGGAGAAAAGATGAAAGTTCTAGAAGA…
```

B. LynA sequence in LynA^{KO}(CRISPR)

DNA notation (connecting mRNA splice junctions)

```
WT  ATGGGATGTATTAAATCAAAAAGGAAAGACAATCTCAATGACGATGAAGTAGATTCGAAGACTCAACCAGTACGTAATACT
AKO ATGGGATGTATTAAATCAAAAAGGAAAGACAATCTCAATGACGATGAAGTAGATTCGAAGACTCAACCAGTACGTAATACT
    **********************************************************************************

WT  GACCGAACTATTTATGTGAGAGATCCAACGTCCAATAAACAGCAAAGGCCAGTTCCTGAATTTCATCTTTTACCAGGACAG
AKO GACCGAACAGAGAC-------------------------------------GTTCCTGAATTTCATCTTTTACCAGGACAG
    ********                                            ****************************

WT  GATTTCAAACAAAAG ATCCAGAGGAACAAGGTGACATTGTGGTGGCCTTATACCCTTATGATGGCATCCACCCAGATGAC
AKO GATTTCAAACAAAAG ATCCAGAGGAACAAGGTGA(putative PTC)
    **********************************
```

C. LynB sequence in LynA^{KO}(CRISPR)

DNA notation (connecting mRNA splice junctions)

```
WT  ATGGGATGTATTAAATCAAAAAGGAAAGACAATCTCAATGACGATGAAGTAGATTCGAAGACTCAACCAGTTCCTGAATTT…
AKO ATGGGATGTATTAAATCAAAAAGGAAAGACAATCTCAATGACGATGAAGTAGATTCGAAGACTCAACCAGTTCCTGAATTT…
    **********************************************************************************
```

Translation

```
WT  MGCIKSKRKDNLNDDEVDSKTQPVPEFHLLPGQRFQTKDPEEQGDIVVALYPYDGIHPDDLSFKKGEKMKVLE…
AKO MGCIKSKRKDNLNDDEVDSKTQPVPEFHLLPGQRFQTKDPEEQGDIVVALYPYDGIHPDDLSFKKGEKMKVLE…
    **********************************************************************
    1                                                                    73
```

Fig. S1. Nucleotide and protein sequence of LynA^{KO}(CRISPR). (A) Genomic sequence of exon 2 (yellow) and exon 3 (green) of murine *Lyn*, illustrating the LynB splice site (boxed) and LynA unique-region insert (cyan). **(B)** WT and LynA^{KO}(CRISPR) (AKO) sequences. The LynA^{KO}(CRISPR) sequence has a frameshift after codon 30 and a putative premature termination codon (PTC) 78, which should induce NMD of the LynA splice product. Nucleotide sequences are shown in DNA notation for ease of comparison to genomic sequence above. **(C)** The RNA and translated protein sequence of LynB is unaffected. Generated with EMBL-EBI Clustal Omega and ExPASy Translate Tool.

LynA sequence in LynB^{KO}(CRISPR)

DNA notation (connecting mRNA splice junctions)

```
WT   ATGGGATGTATTAAATCAAAAAGGAAAGACAATCTCAATGACGATGAAGTAGATTCGAAGACTCAACCAGTACGTAATACTG
BKO  ATGGGATGTATTAAATCAAAAAGGAAAGACAATCTCAATGACGATGAAGTAGATTCGAAGACTCAACCACTGCGTAATACTG
     ************************************************************************ * **********

WT   ACCGAACTATTTATGTGAGAGATCCAACGTCCAATAAACAGCAAAGGCCAGTTCCTGAATTTCATCTTTTACCAGGACAGA…
BKO  ACCGAACTATTTATGTGAGAGATCCAACGTCCAATAAACAGCAAAGGCCAGTTCCTGAATTTCATCTTTTACCAGGACAGA…
     ********************************************************************************
```

Translation

```
WT   MGCIKSKRKDNLNDDEVDSKTQPVRNTDRTIYVRDPTSNKQQRPVPEFHLLPGQRFQTKDPEEQGDIVVALYPYDGIHPDD…
BKO  MGCIKSKRKDNLNDDEVDSKTQPLRNTDRTIYVRDPTSNKQQRPVPEFHLLPGQRFQTKDPEEQGDIVVALYPYDGIHPDD…
     ********************************************************************************
     1                                                                              81
```

(**no LynB due to ablation of splice donor**)

Fig. S2. Nucleotide and protein sequence of LynB^{KO}(CRISPR). LynB is not expressed in the LynB^{KO} due to a splice-site mutation. LynA has a V24L substitution.

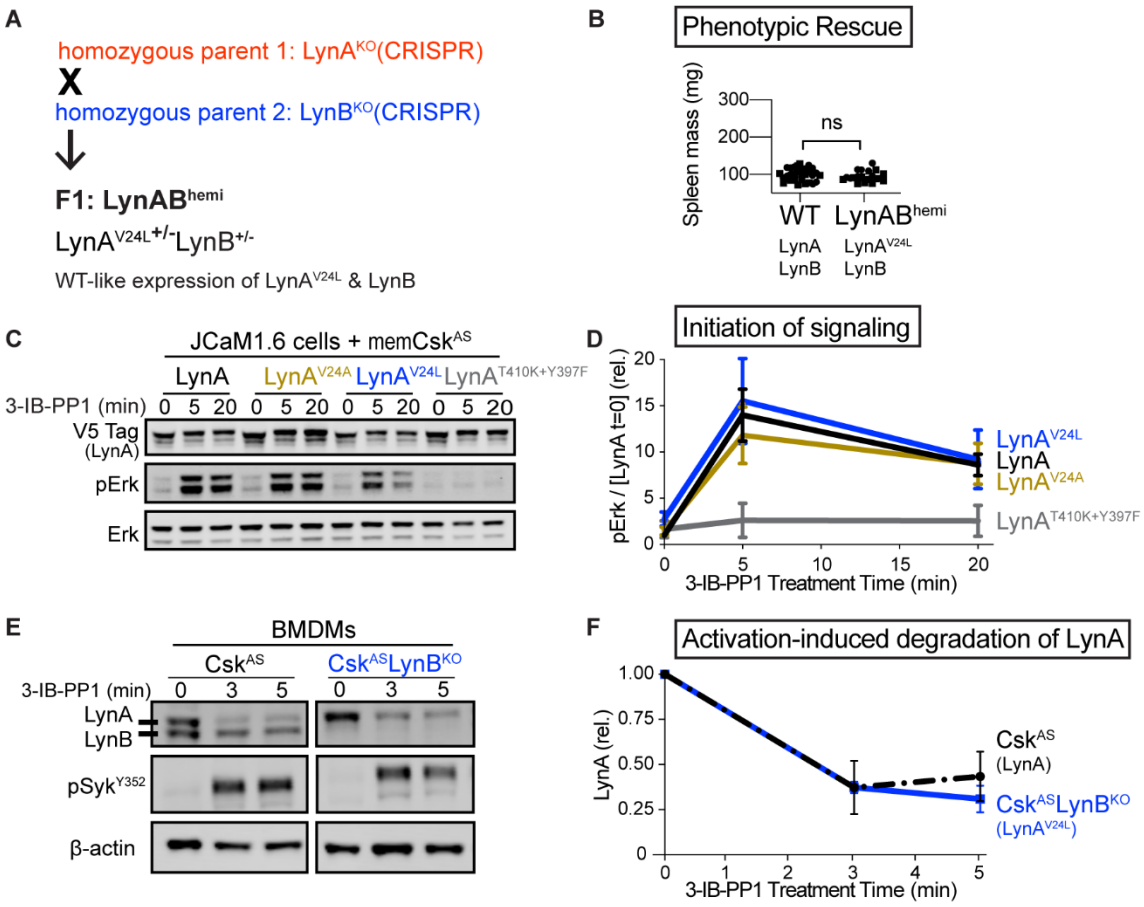

Fig. S3. V24L substitution does not impair LynA function. (A) Lyn protein expression in parental and LynAB^{hemi} mice. **(B)** Phenotypic identity of LynA^{V24L}-expressing LynAB^{hemi} and WT mouse spleens at 8.5 months. **(C)** We have previously shown that ectopic expression of LynA in Lck-deficient JCaM1.6 T cells can restore SFK-dependent ITAM signaling. Treatment of an inhibitor-sensitized variant of the SFK negative regulator Csk (memCsk^{AS}) with the designer inhibitor 3-IB-PP1 induces LynA activation and signal initiation. Representative immunoblots from JCaM1.6 lysates show that WT LynA, LynA^{V24A}, or LynA^{V24L}, but not kinase-dead LynA$^{T410K+Y397F}$ are capable of initiating signaling that leads to Erk1/2 phosphorylation (pT202/pY204); total Erk reflects protein loading. **(D)** Quantification of Lyn-dependent Erk phosphorylation during 3-IB-PP1 treatment, corrected for the relative levels of transfected LynA protein. **(E)** We generated Csk^{AS}LynB^{KO} mice, which expressed LynA^{V24L} and the Csk^{AS}-transgene, and activated the SFKs in Csk^{AS}LynB^{KO} BMDMs by treating with 3-IB-PP1. Representative immunoblots show loss of LynA and increased phosphorylation of Syk (pY352) upon SFK activation; β-actin reflects protein loading. **(F)** Rates of degradation of WT LynA and LynA^{V24L} are indistinguishable, indicating that the V24L substitution does not impair Y32 phosphorylation, interaction with c-Cbl, or other signal-initiation or regulatory machinery.

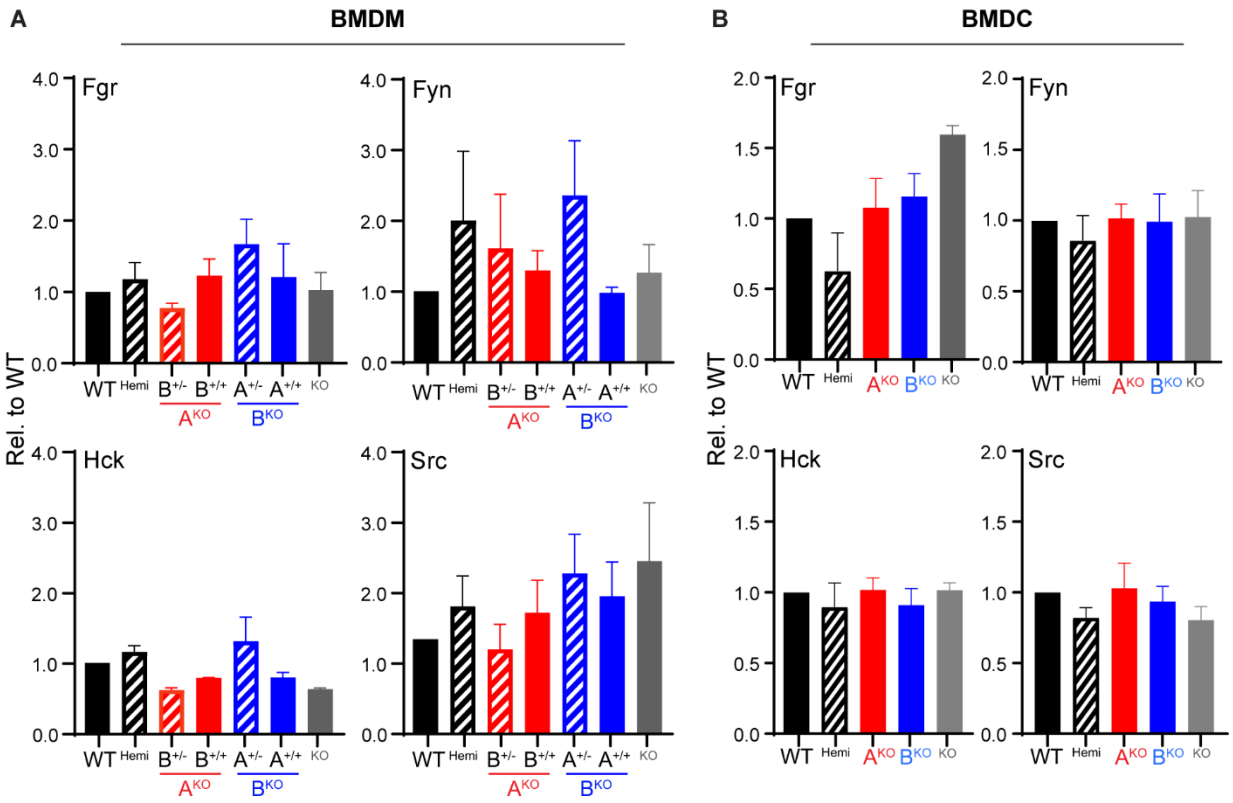

Fig. S4. SFK expression is largely unaltered in LynA^{KO} and LynB^{KO} BMDMs and BMDCs. **(A)** Immunoblot quantification of total Fgr, Fyn, Hck, and Src protein levels in Lyn-knockout BMDMs relative to WT. **(B)** Quantification of SFKs in BMDCs. For both panels error is reported as SEM (n=3-5). No significance was found with one-way ANOVA with Tukey's multiple comparison test except [BMDC Fgr, Lyn^{KO}] P=0.017.

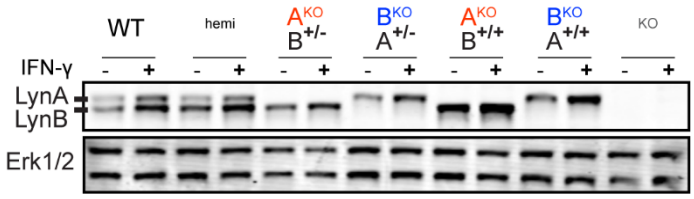

Fig. S5. Lyn upregulation in response to IFN-γ is preserved in LynA^{KO} and LynB^{KO} BMDMs. Representative immunoblot showing Lyn protein expression in WT and Lyn knockout BMDMs rested (-) or incubated overnight with low-dose IFN-γ (+).

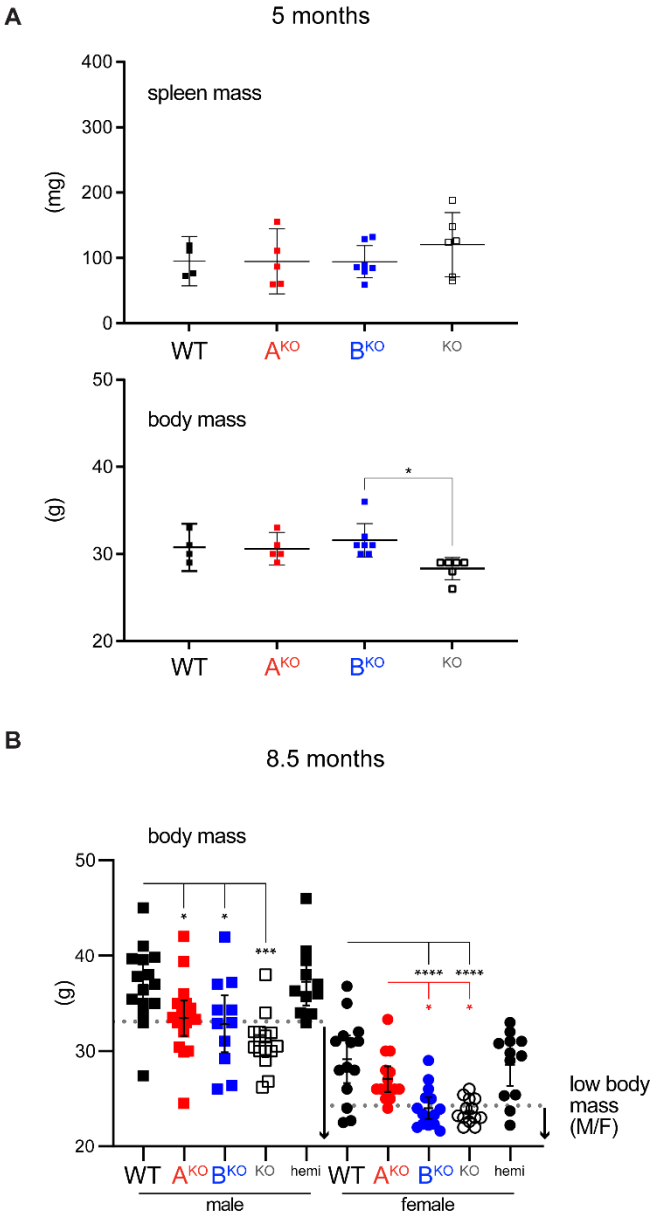

Fig. S6. No splenomegaly in 5-month-old mice and variable body mass in 8.5-month-old mice. (A) Spleen and body masses in male sentinel mice aged 5 months, with incomplete progression to severe disease; error bars: 95% CI. **(B)** Body masses of 8.5-month-old mice from **Fig.3**, with dotted lines reflecting low-mass cutoffs for males (M < 33.2 g) and females (F < 24.5 g).

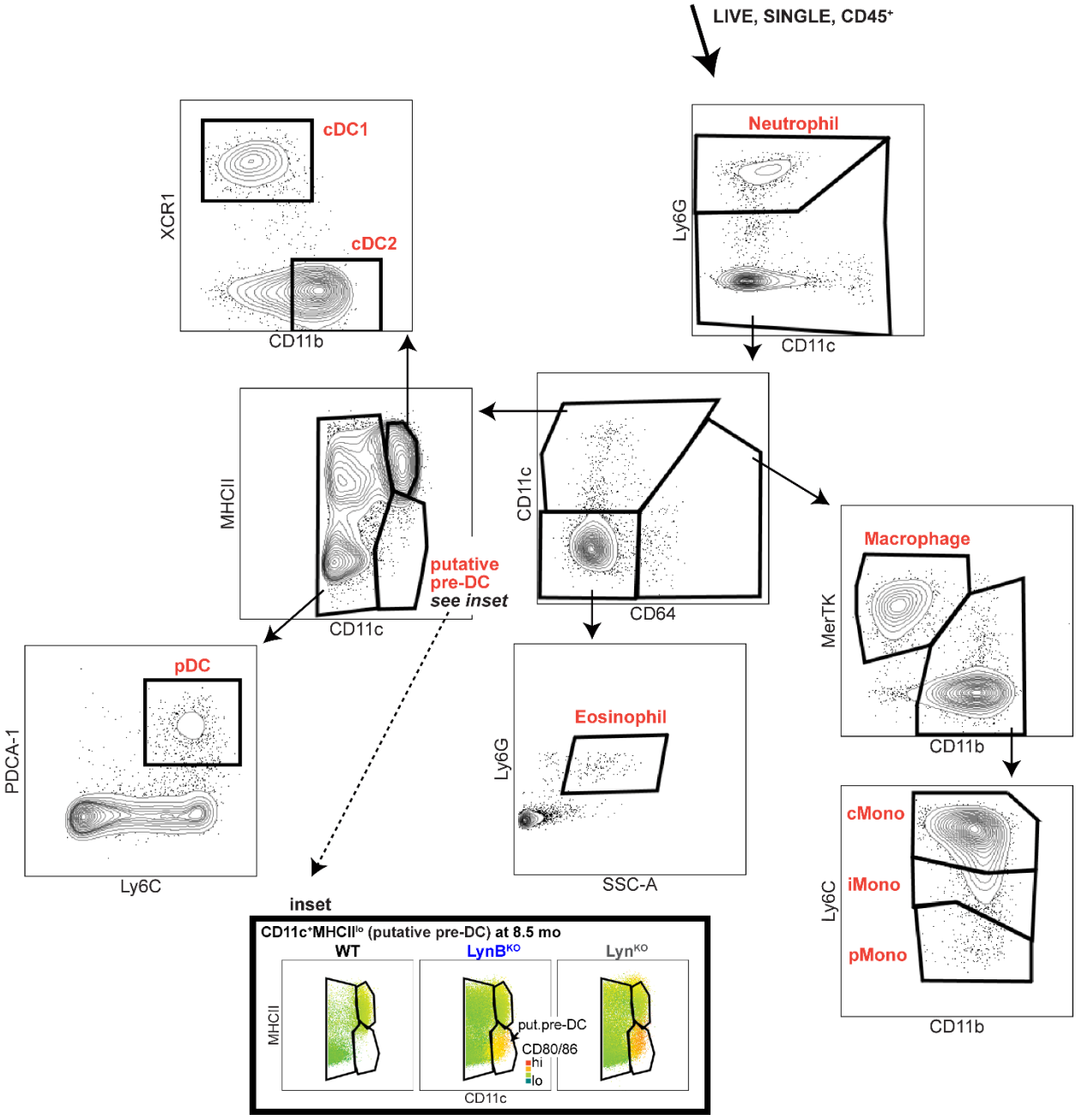

Fig. S7. Myeloid Gating. Live, single, hematopoietic ($CD45^{+}$) cell gating, showing spleen subsetting of a representative WT mouse. End-gate population assignments are highlighted in orange. $CD11c^{hi}SiglecF^{-}MHCII^{lo}$ expression is consistent with a pre-DC population. **Inset:** $CD11c^{+}MHCII^{lo}$ putative (put.)pre-DCs in spleen suspensions from WT, $LynB^{KO}$, and Lyn^{KO} mice aged 8.5 months, with CD80/86 expression on a color axis.

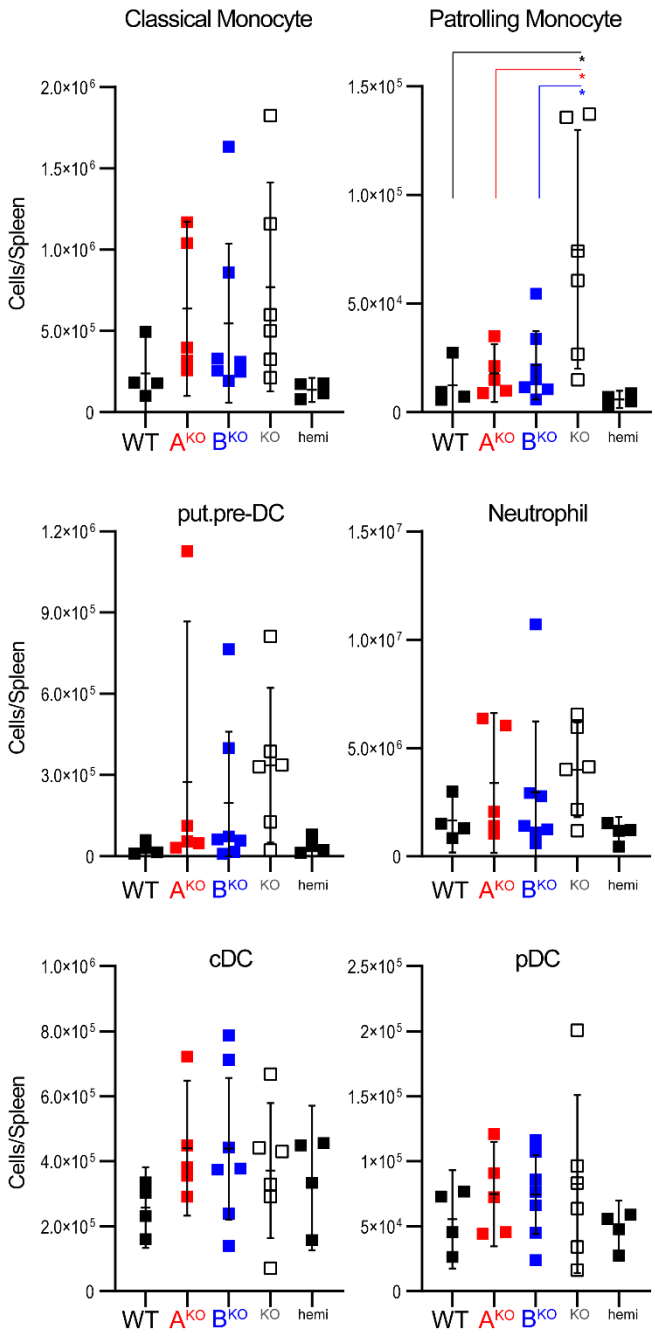

Fig. S8. Splenic myeloid-cell composition at 5 months. Flow cytometry and cell counting methodologies were used to enumerate myeloid cellularity in spleens from 5-month-old mice. No significant differences were found in classical monocyte, neutrophil, putative pre-DC, cDC, or pDC numbers.

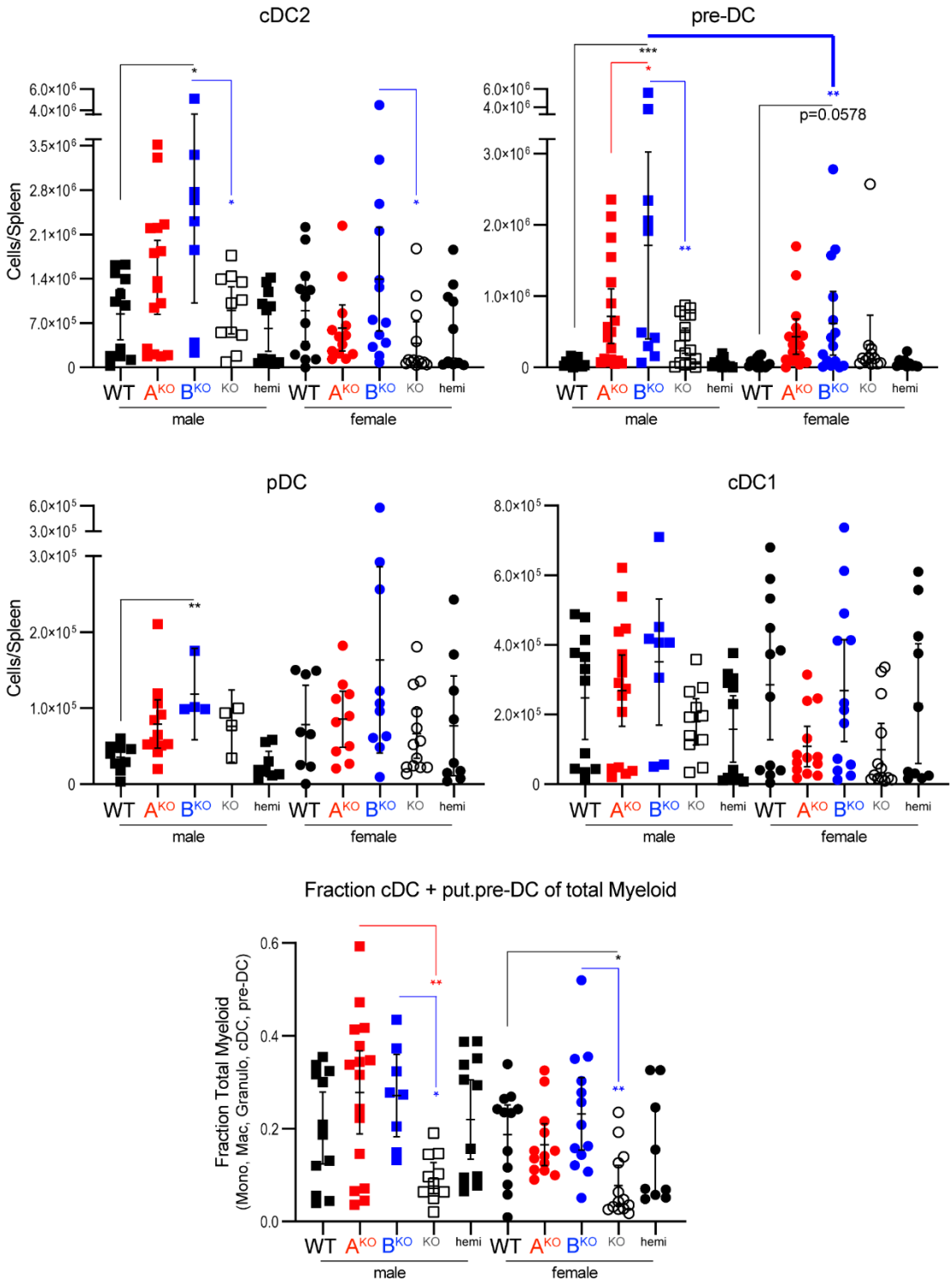

Fig. S9. DC numbers in spleens from 8.5-month-old mice. Total cells per spleen and fractional content of DC populations from mice aged 8.5 months. Error bars: 95% CI. In addition to the annotated comparisons (asterisks colored by genotype), there are no significant differences between LynAB^{hemi} and WT. For clarity, only male/female comparisons within a genotype are shown. Pooled from 4-6 separate analyses.

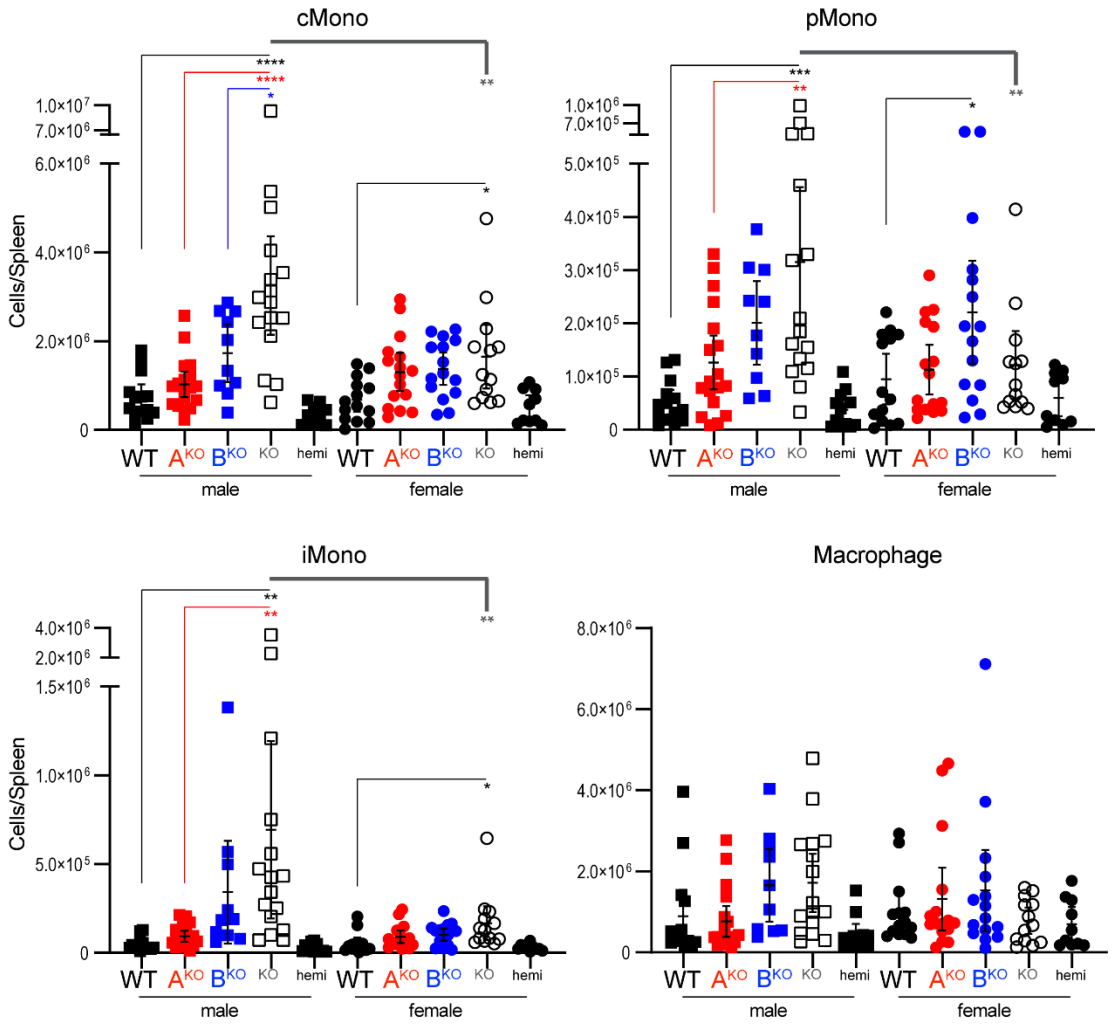

Fig. S10. Monocyte and macrophage populations in spleens from 8.5-month-old mice. Total monocyte and macrophage numbers per spleen in mice aged 8.5 months. Error bars: 95% CI. In addition to the annotated comparisons (asterisks colored by genotype), there are no significant differences between LynAB^{hemi} and WT. For clarity, only male/female comparisons within a genotype are shown. Pooled from 4-6 separate analyses.

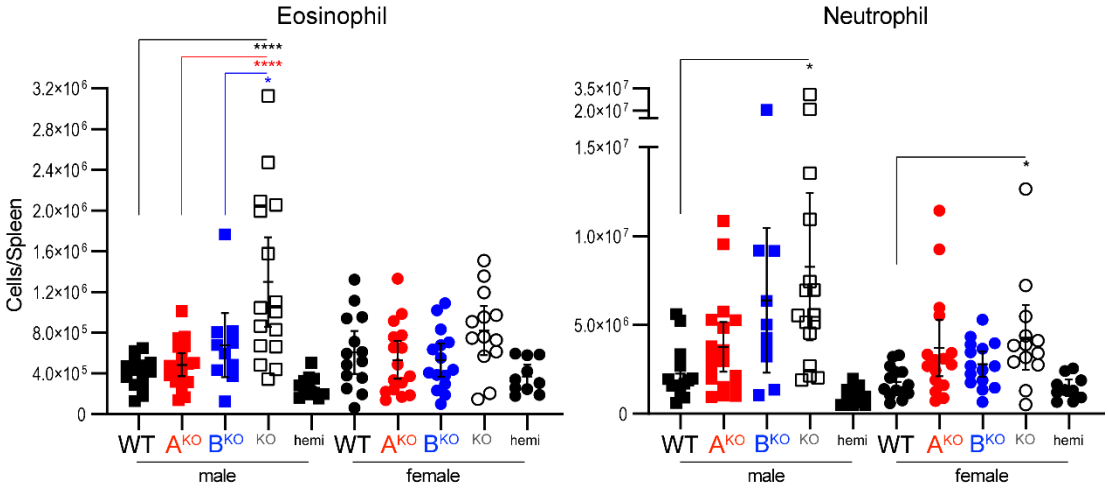

Fig. S11. Granulocyte populations in spleens from 8.5-month-old mice. Total eosinophil and neutrophil numbers per spleen in mice aged 8.5 months. Error bars: 95% CI. In addition to the annotated comparisons (asterisks colored by genotype), there are no significant differences between LynAB^{hemi} and WT. For clarity, only male/female comparisons within a genotype are shown. Pooled from 4-6 separate analyses.

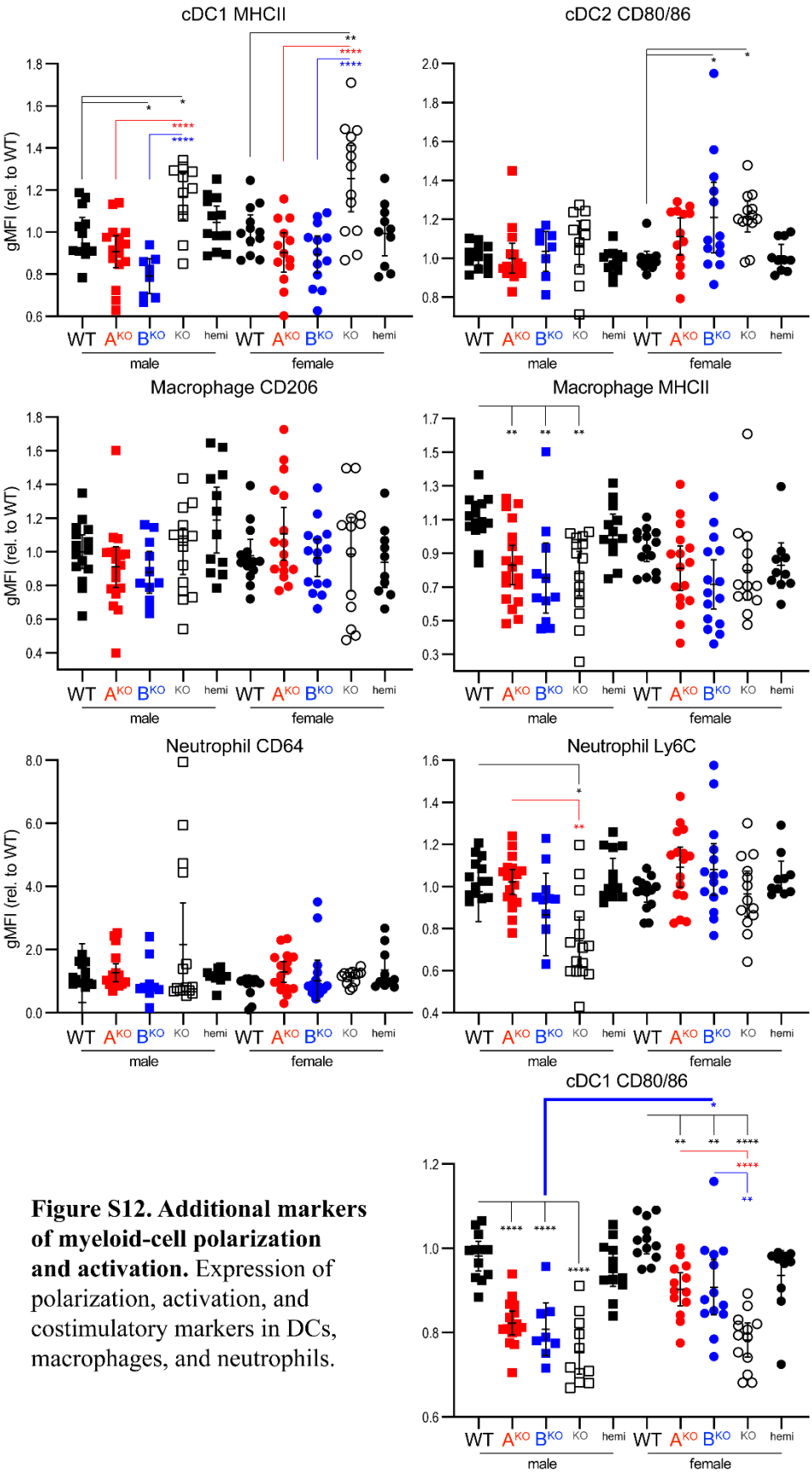

Figure S12. Additional markers of myeloid-cell polarization and activation. Expression of polarization, activation, and costimulatory markers in DCs, macrophages, and neutrophils.

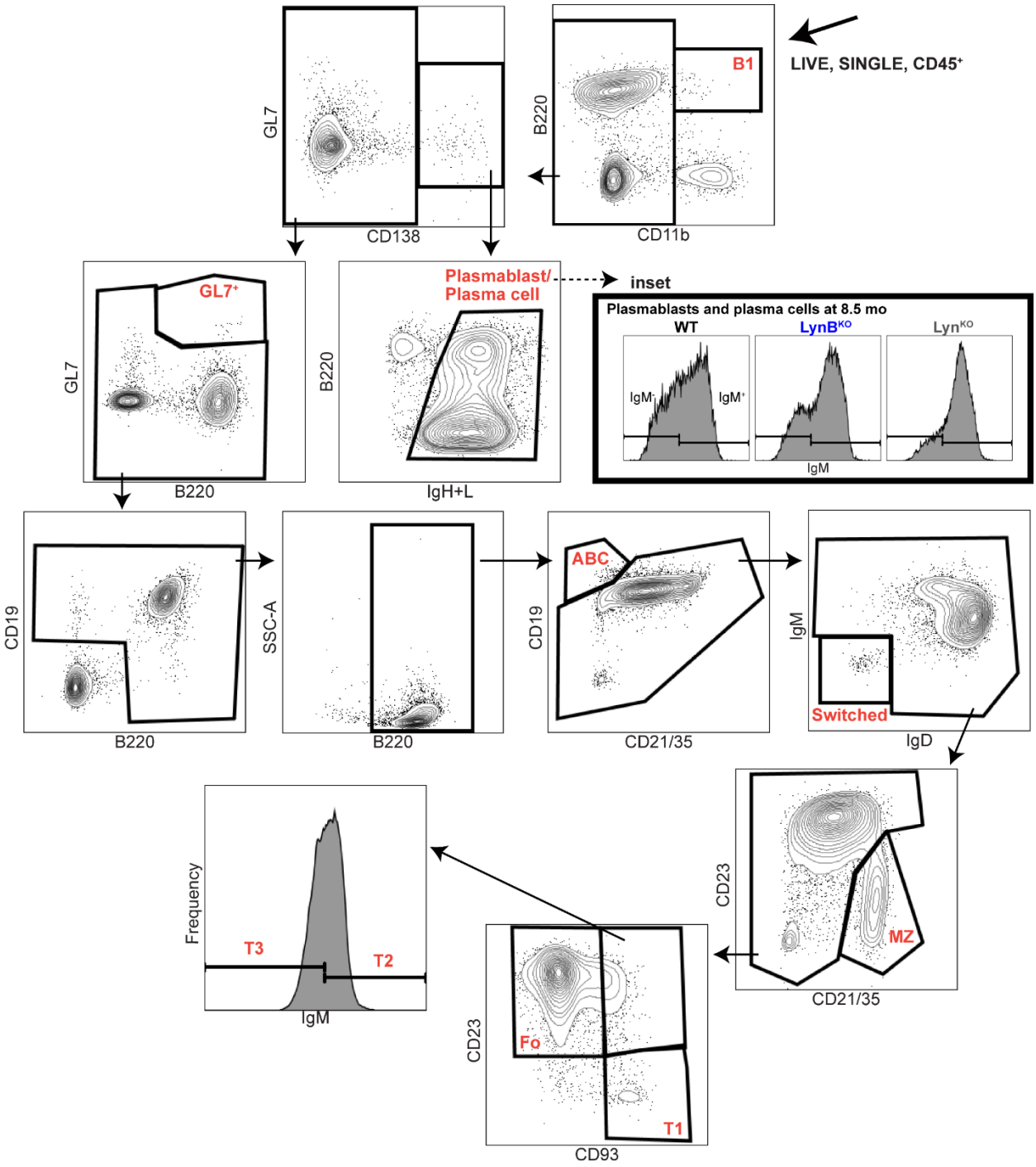

Fig. S13. B-cell Gating. Live, single, hematopoietic ($CD45^{+}$) cell gating, showing spleen subsetting of a representative WT mouse aged 8.5 months. Abbreviations: GL7-expressing germinal-center or activated ($GL7^{+}$) B cell, age-associated B cell (ABC), follicular (Fo) B cell, marginal zone (MZ) B cell, and transitional (T) types 1, 2, and 3 B cell. **Inset:** Expression of IgM by plasmablasts and plasma cells from WT, $LynB^{KO}$, and Lyn^{KO} mice aged 8.5 months.

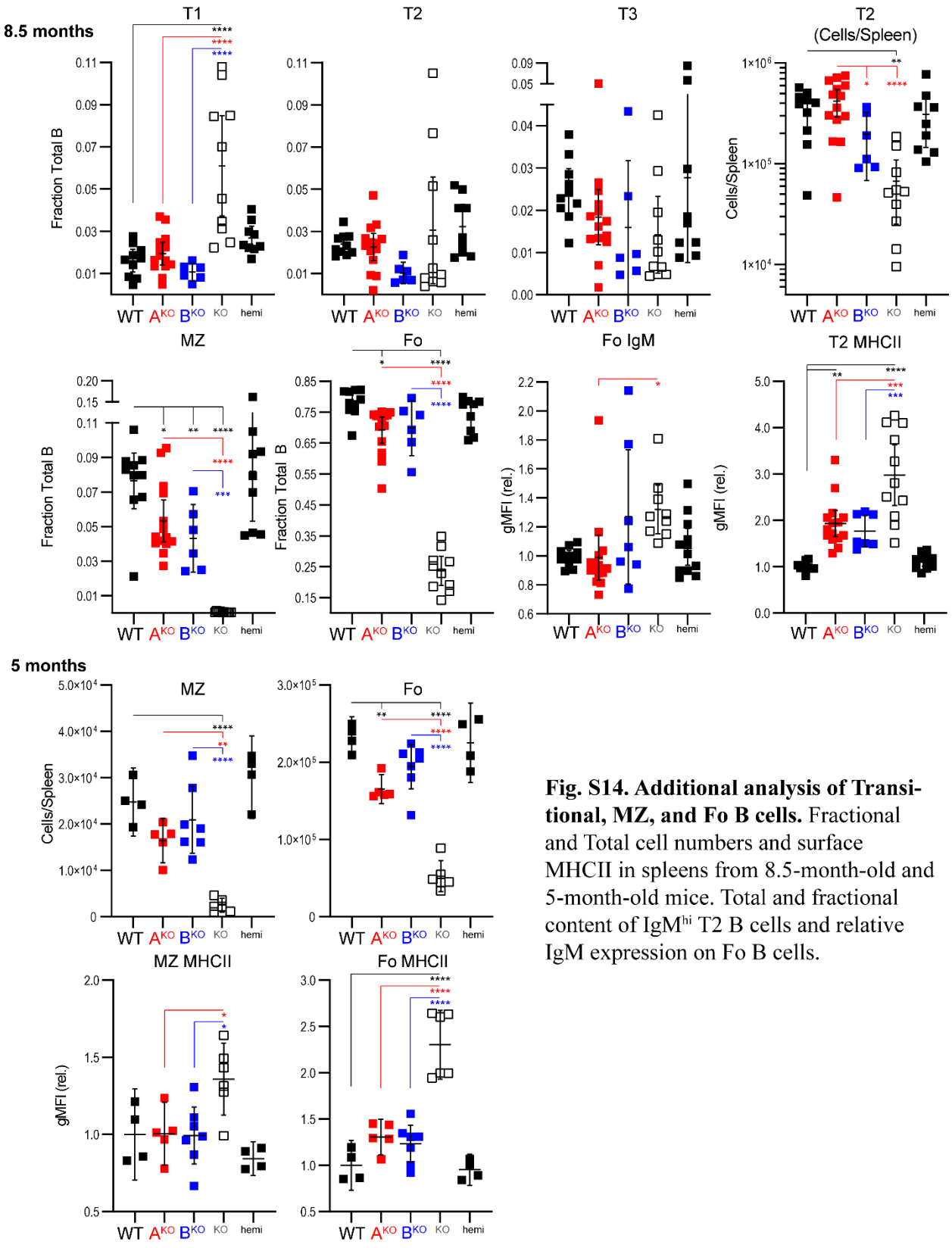

Fig. S14. Additional analysis of Transitional, MZ, and Fo B cells. Fractional and Total cell numbers and surface MHCII in spleens from 8.5-month-old and 5-month-old mice. Total and fractional content of IgM^{hi} T2 B cells and relative IgM expression on Fo B cells.

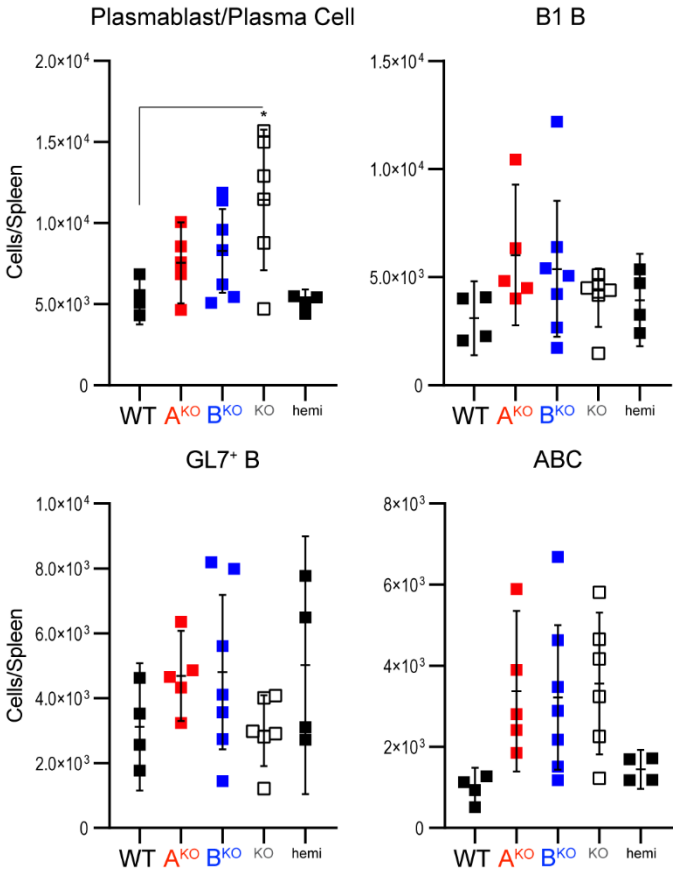

Fig. S15. Splenic B-cell composition at 5 months. Flow cytometry and cell counting were used to enumerate B cellularity in spleens from 5-month-old mice. No significant differences were found in LynA^{KO} or LynB^{KO} relative to WT or total Lyn^{KO}.

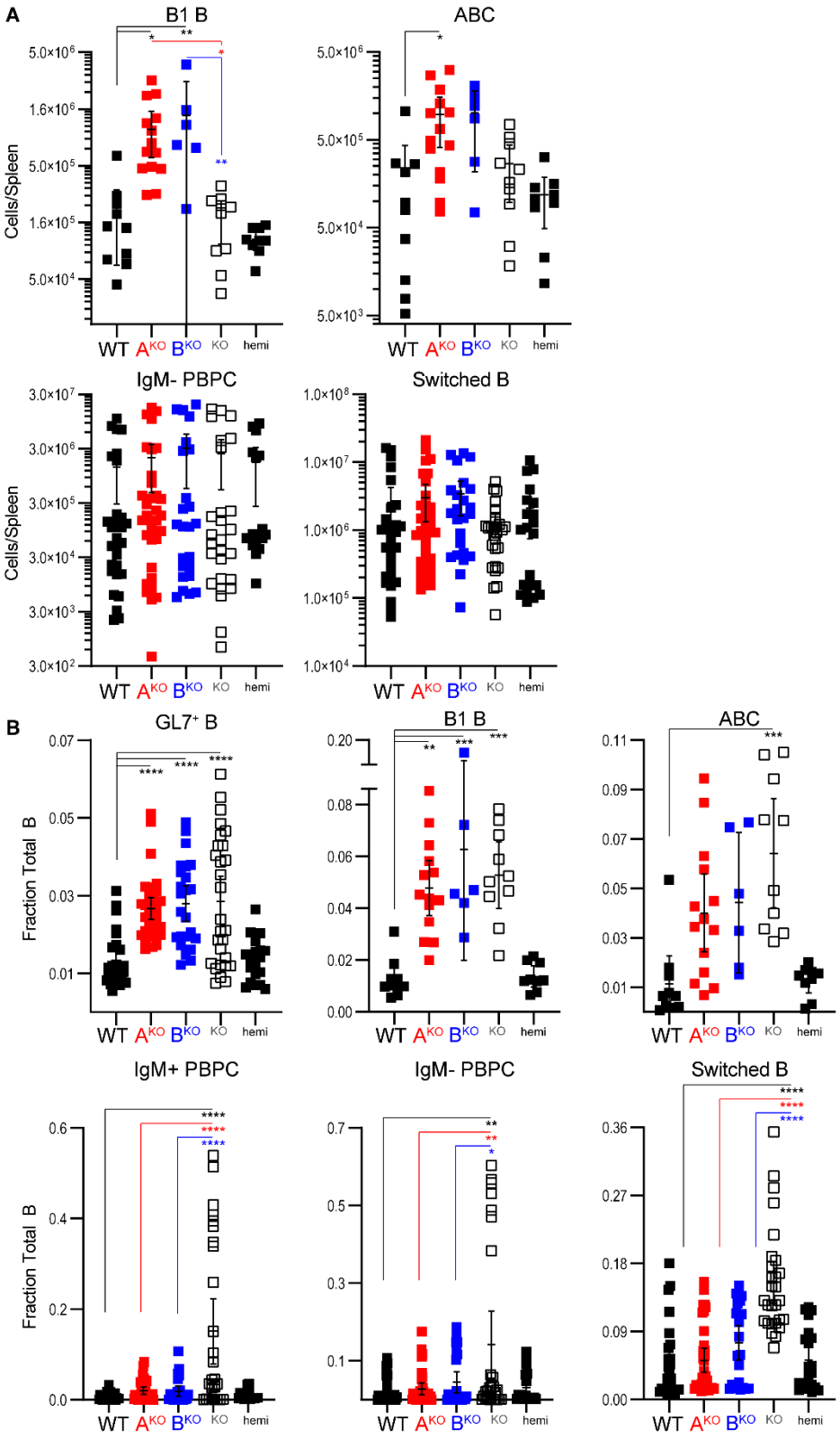

Fig. S16. Differentiated Splenic B cells. (A) Total cells per spleen and **(B)** fractional content of splenic B cells from mice aged 8.5 months. Error: 95% CI. In addition to the annotated comparisons (asterisks colored by genotype), there are no sig. differences between LynAB^{hemi} and WT; 4-6 separate analyses.

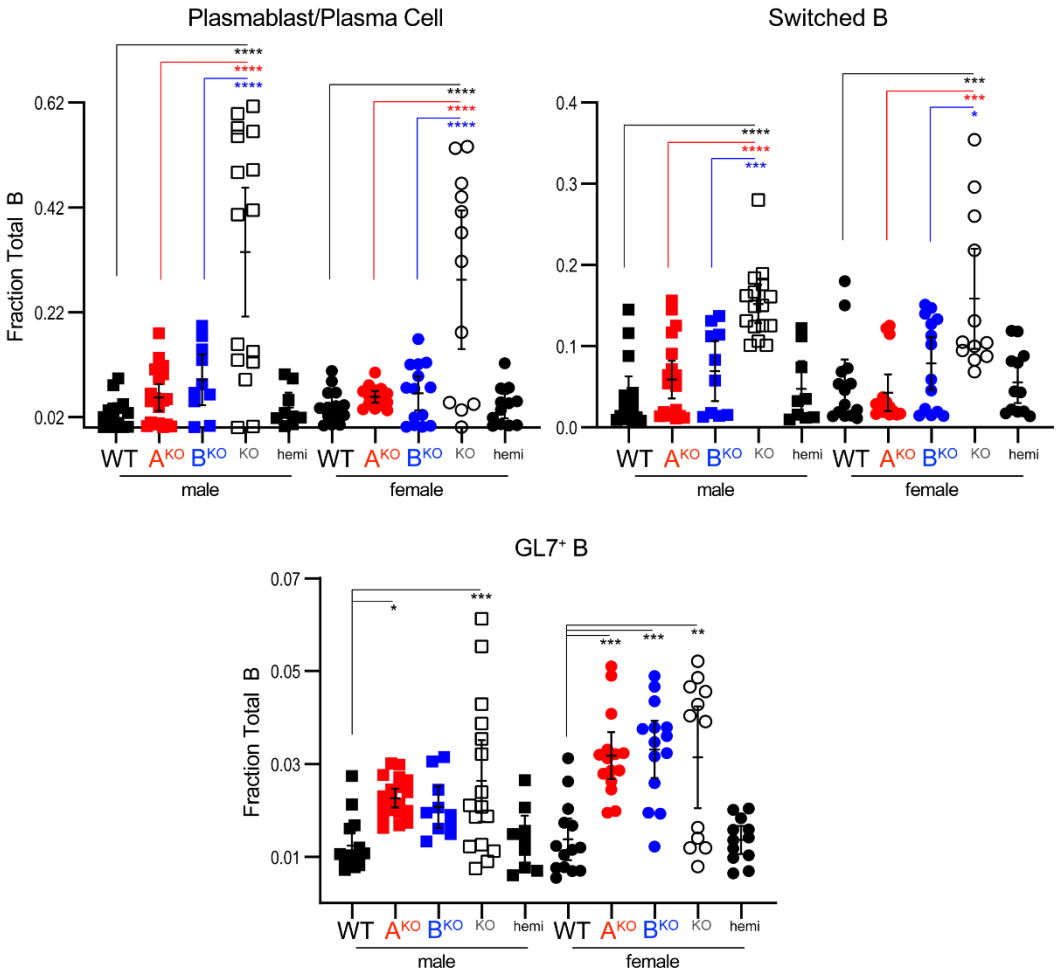

Fig. S17. Representative B-cell populations in 8.5-month-old male and female mice. B1 B cells and ABC analyses were not sufficiently powered to separate by sex but trended similarly to $GL7^+$ cells.

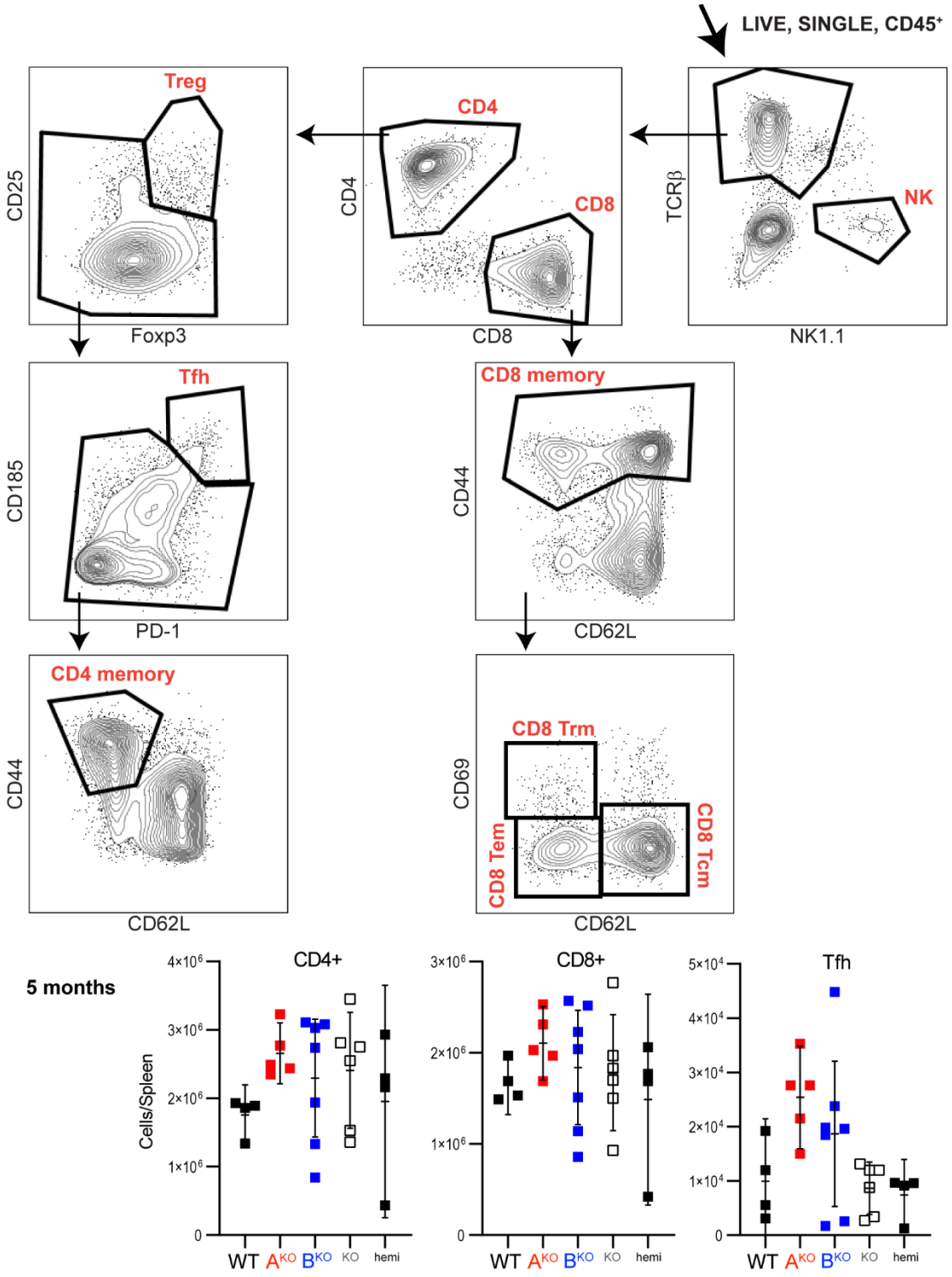

Fig. S18. T-Cell Gating. Live, single, hematopoietic (CD45^{+}) cell gating, showing spleen subsetting of a representative WT mouse aged 8.5 months. Abbreviations: regulatory T (Treg), CD8 T-resident memory (Trm), T follicular helper (Tfh), and T resident memory (Trm), T effector memory (Tem), and T central memory (Tcm). No sig. differences at 5 months.

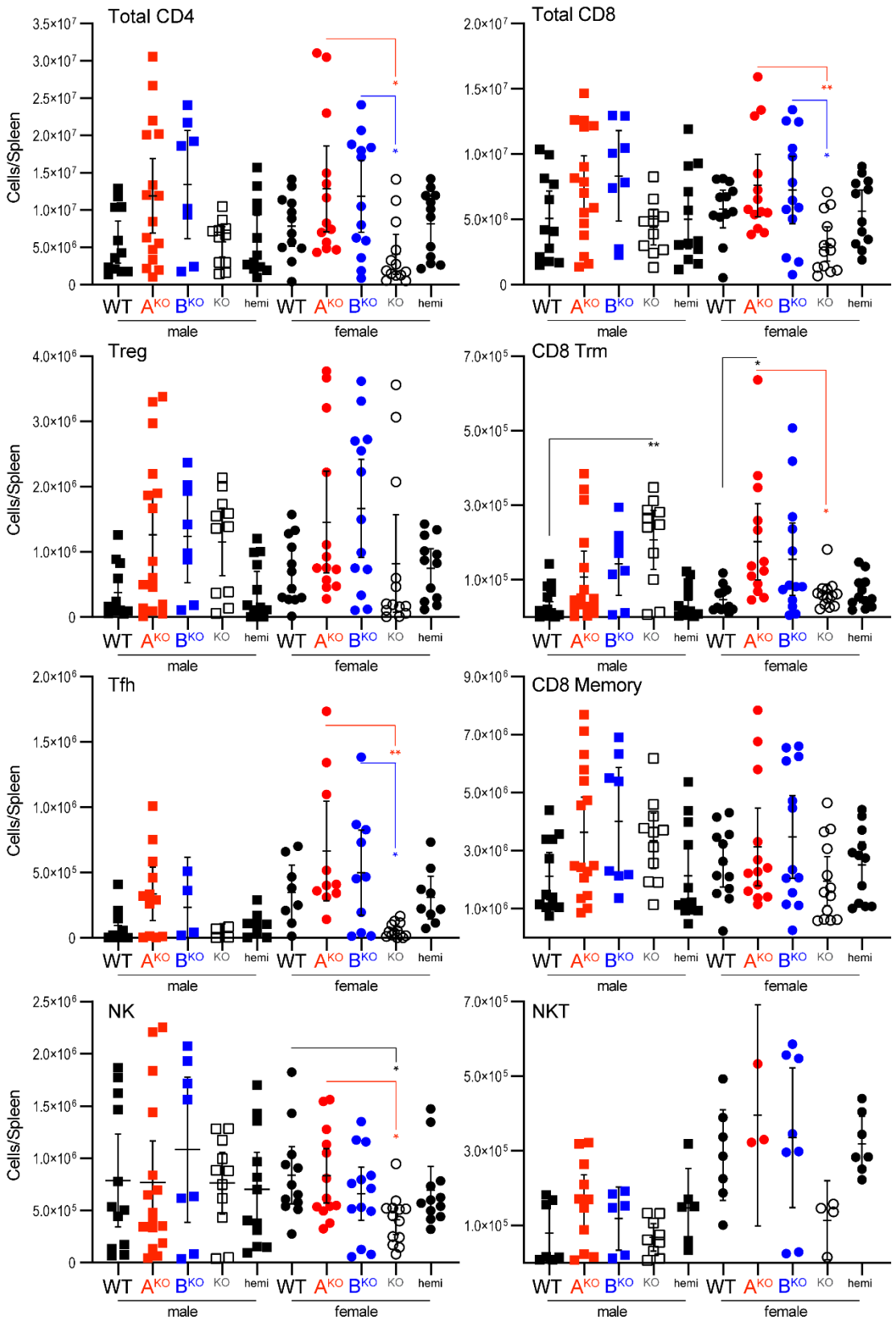

Fig. S19. T-cell and NK-cell populations in spleens from 8.5-month-old mice.

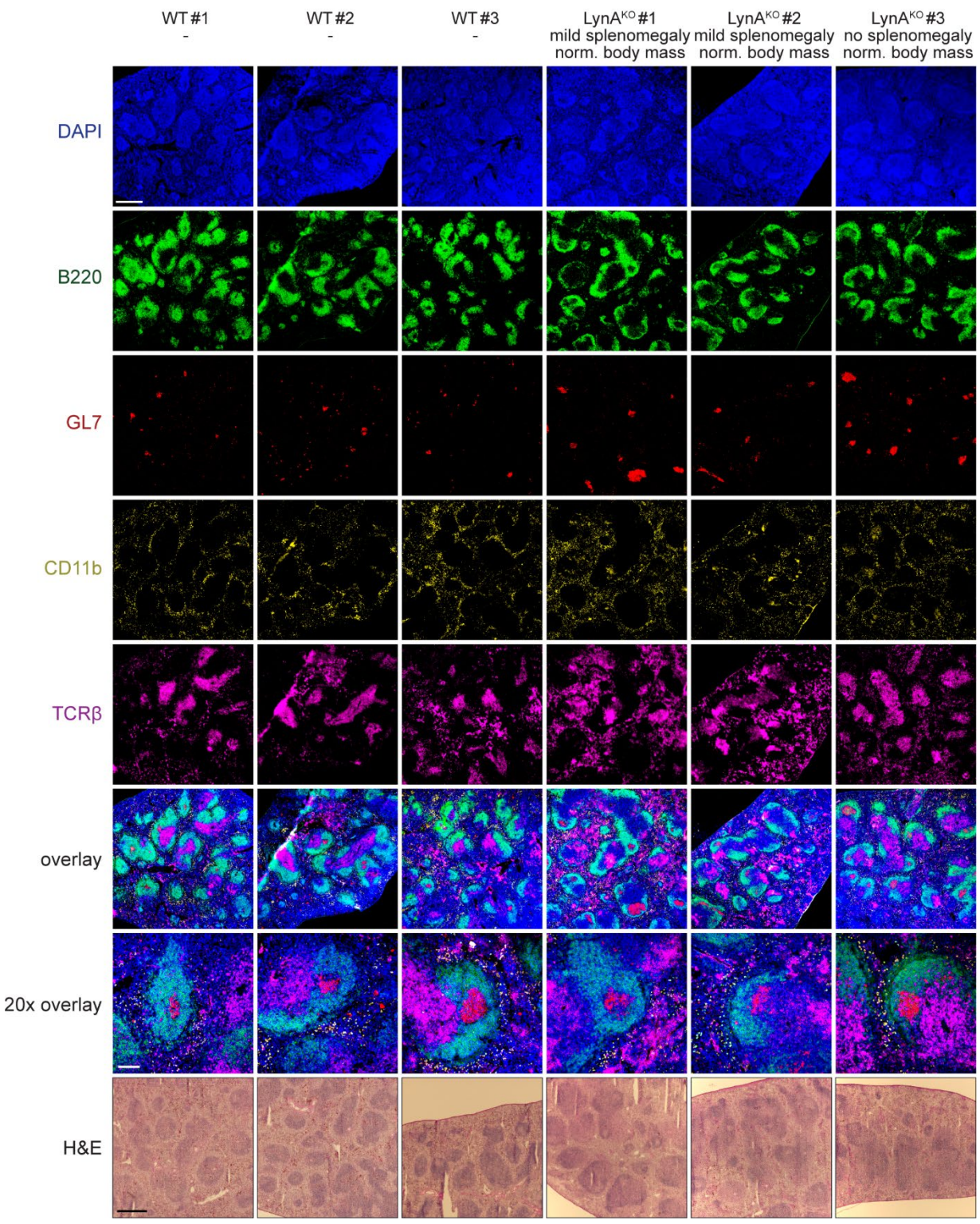

Fig. S20. Additional spleen images from WT and LynA^{KO} mice. Immunofluorescence images of spleens from different individual WT and LynA^{KO} mice, with corresponding splenomegaly or low body mass, as defined in Fig. 3. WT 2F+1M, LynA^{KO} 3F.

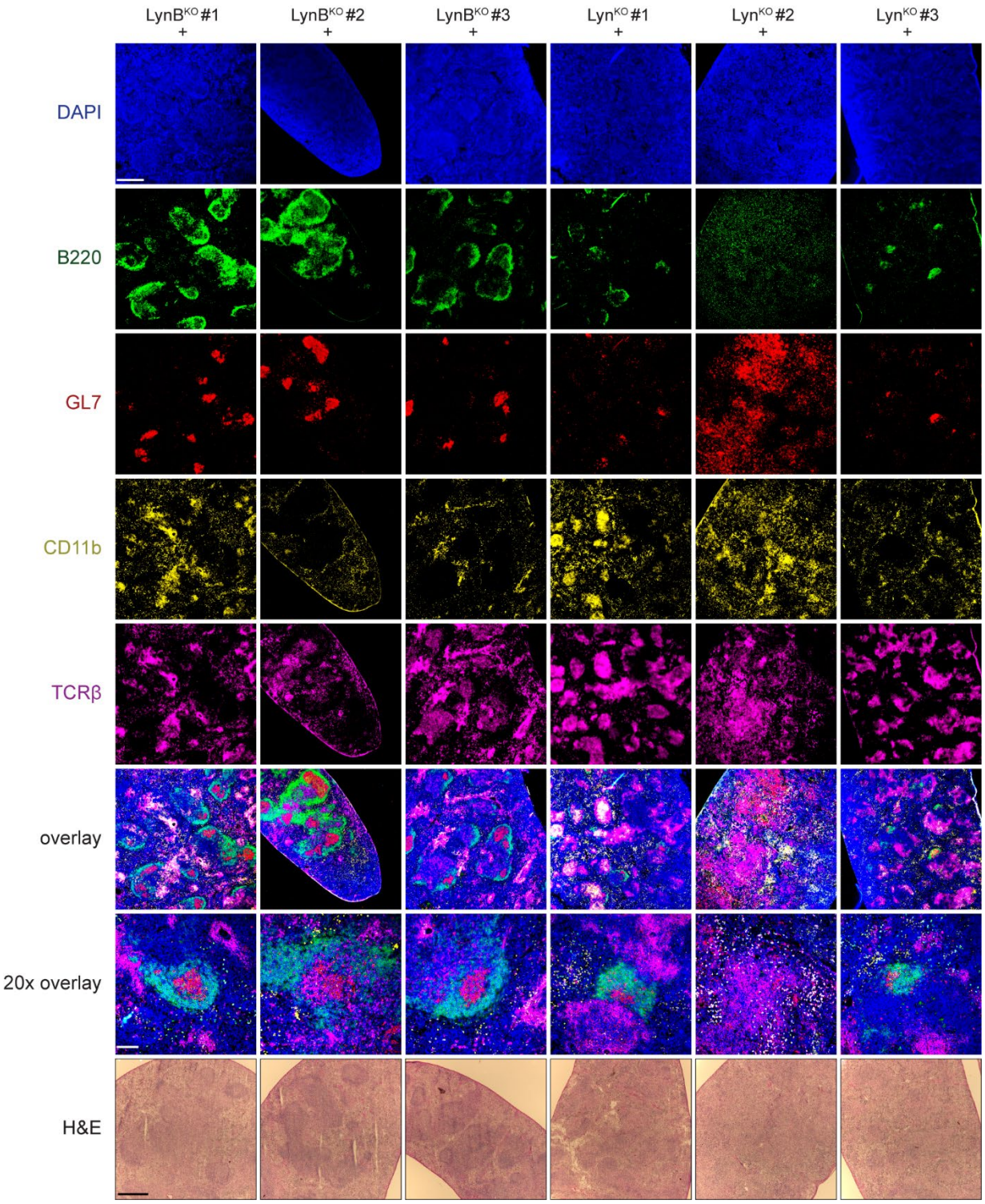

Fig. S21. Additional spleen images from LynB^{KO} and Lyn^{KO} mice. Immunofluorescence images of spleens from different individual LynB^{KO} and Lyn^{KO} mice, with corresponding splenomegaly or low body mass, as defined in Fig. 3. LynB^{KO} 3F, Lyn^{KO} 3M.